

Fifteen new T dwarfs discovered in the UKIDSS Large Area Survey

D. J. Pinfield,^{1*} B. Burningham,¹ M. Tamura,² S. K. Leggett,³ N. Lodieu,⁴
 P. W. Lucas,¹ D. J. Mortlock,⁵ S. J. Warren,⁵ D. Homeier,⁶ M. Ishii,⁷ N. R. Deacon,⁸
 R. G. McMahon,⁹ P. C. Hewett,⁹ M. R. Zapatero Osori,⁴ E. L. Martin,⁴
 H. R. A. Jones,¹ B. P. Venemans,⁹ A. C. Day-Jones,¹ P. D. Dobbie,¹⁰ S. L. Folkes,¹
 S. Dye,¹¹ F. Allard,¹² I. Baraffe,¹³ D. Barrado y Navascués,¹⁴ S. L. Casewell,¹⁵
 K. Chiu,¹⁶ G. Chabrier,¹³ F. Clarke,¹⁷ S. T. Hodgkin,⁹ A. Magazzù,¹⁸
 M. J. McCaughrean,¹⁶ T. Nakajima,² Y. Pavlenko¹⁹ and C. G. Tinney²⁰

¹Centre for Astrophysics Research, Science and Technology Research Institute, University of Hertfordshire, Hatfield AL10 9AB

²National Astronomical Observatory, Mitaka, Tokyo 181-8588, Japan

³Gemini Observatory, 670 N. A'ohoku Place, Hilo, HI 96720, USA

⁴Instituto de Astrofísica de Canarias, 38200 La Laguna, Spain

⁵Astrophysics Group, Imperial College London, Blackett Laboratory, Prince Consort Road, London SW7 2AZ

⁶Institut für Astrophysik, Georg-August-Universität, Friedrich-Hund-Platz 1, 37077 Göttingen, Germany

⁷Subaru Telescope, 650 North A'ohoku Place, Hilo, HI 96720, USA

⁸Department of Astrophysics, Faculty of Science, Radboud University Nijmegen, PO Box 9010, 6500 GL Nijmegen, The Netherlands

⁹Institute of Astronomy, Madingley Road, Cambridge CB3 0HA

¹⁰Anglo-Australian Observatory, PO Box 296, Epping 1710, Australia

¹¹Cardif University, School of Physics & Astronomy, Queens Buildings, The Parade, Cardiff CF24 3AA

¹²Centre de Recherche Astrophysique de Lyon, UMR5574, CNRS, Université de Lyon, Ecole Normale Supérieure, 46 Allée d'Italie, F-69364 Lyon Cedex 07, France

¹³C.R.A.L. (UMR 5574 CNRS), Ecole Normale Supérieure, F-69364 Lyon Cedex 07, France

¹⁴Laboratorio de Astrofísica Espacial y Física Fundamental, INTA, PO Box 50727, E-2808 Madrid, Spain

¹⁵Department of Physics and Astronomy, University of Leicester, University Road, Leicester LE1 7RH

¹⁶School of Physics, University of Exeter, Stocker Road, Exeter, Devon EX4 4QL

¹⁷European Southern Observatory, Alonso de Cordova 3107, Casilla 19001, Santiago 19, Chile

¹⁸Fundación Galileo Galilei-INAf, Apartado 565, E-38700 Santa Cruz de La Palma, Spain

¹⁹Main Astronomical Observatory, National Academy of Sciences, Zabolotnoho 27, Kyiv-127 03680, Ukraine

²⁰Department of Astrophysics, University of New South Wales, Sydney, NSW 2052, Australia

Accepted 2008 July 18. Received 2008 July 17; in original form 2008 April 14

ABSTRACT

We present the discovery of 15 new T2.5–T7.5 dwarfs (with estimated distances ~ 24 –93 pc), identified in the first three main data releases of the United Kingdom Infrared Telescope (UKIRT) Infrared Deep Sky Survey. This brings the total number of T dwarfs discovered in the Large Area Survey (LAS) (to date) to 28. These discoveries are confirmed by near-infrared spectroscopy, from which we derive spectral types on the unified scheme of Burgasser et al. Seven of the new T dwarfs have spectral types of T2.5–T4.5, five have spectral types of T5–T5.5, one is a T6.5p and two are T7–7.5. We assess spectral morphology and colours to identify T dwarfs in our sample that may have non-typical physical properties (by comparison to solar neighbourhood populations), and find that three of these new T dwarfs may have unusual metallicity, two may have low surface gravity, and one may have high surface gravity. The colours of the full sample of LAS T dwarfs show a possible trend to bluer $Y - J$ with decreasing effective temperature, and some interesting colour changes in $J - H$ and $z - J$ (deserving further investigation) beyond T8. The LAS T dwarf sample from the first and second main data releases show good evidence for a good level of completion to $J = 19$. By accounting for the main sources of incompleteness (selection, follow-up and spatial) as well as the effects of unresolved binarity, Malmquist and Eddington bias, we estimate that

*E-mail: D.J.Pinfield@herts.ac.uk

there are $17 \pm 4 \geq T 4$ dwarfs in the $J \leq 19$ volume of the LAS second data release. This value is most consistent with theoretical predictions if the substellar mass function exponent α ($dN/dm \propto m^{-\alpha}$) lies between -1.0 and 0 . This is consistent with the latest 2-Micron All Sky Survey (2MASS)/Sloan Digital Sky Survey (SDSS) constraint (which is based on lower number statistics) and is significantly lower than the $\alpha \sim 1.0$ suggested by L dwarf field populations, which is possibly a result of the lower mass range probed by the T dwarf class.

Key words: techniques: photometric – techniques: spectroscopic – surveys – stars: low-mass, brown dwarfs – infrared: stars.

1 INTRODUCTION

The advent of the large-scale Sloan Digital Sky Survey (SDSS; York et al. 2000), the 2-Micron All Sky Survey (2MASS; Skrutskie et al. 2006) and the Deep Near-Infrared Survey of the Southern Sky (DENIS; Epchtein et al. 1997) were the main factors that led to the identification and study of the two spectral classes beyond M: the L dwarfs (with effective temperatures $T_{\text{eff}} \sim 2300\text{--}1450$ K, from parallax distance and bolometric flux constraints; e.g. Dahn et al. 2002; Golimowski et al. 2004) have dusty atmospheres and very red near-infrared colours, while the even cooler T dwarfs ($T_{\text{eff}} < 1450$ K; e.g. Tinney, Burgasser & Kirkpatrick 2003; Vrba et al. 2004) have clear atmospheres (from which the dust has settled), and their blue infrared spectra are dominated by strong CH_4 and H_2O absorption bands. The spectral typing scheme of Kirkpatrick et al. (1999) established the first properly classified L dwarf population via 2MASS discoveries. The first T dwarf was discovered as a close companion to the early M dwarf Gl 229 (Nakajima et al. 1995), and the first L dwarf as a companion to the white dwarf GD 165 (Becklin & Zuckerman 1988; Kirkpatrick, Henry & Liebert 1993). However, the subsequent growth of the known T (and L) dwarf populations (>500 L dwarfs and >100 T dwarfs are now known; e.g. Kirkpatrick 2005) has been predominantly achieved via searches of the SDSS (e.g. Leggett et al. 2000b; Geballe et al. 2002; Knapp et al. 2004; Chiu et al. 2006) and 2MASS (e.g. Kirkpatrick et al. 2000; Burgasser et al. 2002, 2004; Tinney et al. 2005; Cruz et al. 2007; Looper, Kirkpatrick & Burgasser 2007) data bases.

The coolest T_{eff} probed by SDSS and 2MASS are currently defined by the eight T7.5–8 dwarfs (as typed by the Burgasser et al. 2006b, hereafter B06) discovered in these surveys. These objects have T_{eff} in the range 725–950 K (Geballe et al. 2001; Burgasser et al. 2006c; Saumon et al. 2006, 2007; Leggett et al. 2007). At lower T_{eff} it is possible that a new spectral class (pre-emptively called Y, following Kirkpatrick et al. 1999) may be necessary, if for example spectral changes occur such as the strengthening of ammonia absorption, and/or the condensation of atmospheric water clouds (Burrows, Sudarsky & Lunine 2003). L and T dwarfs already encompass the temperature scale of transiting ‘hot Jupiters’ (e.g. Knutson et al. 2007), and populating the even cooler T_{eff} regime will allow us to study and understand atmospheres whose T_{eff} is similar to cooler extrasolar giant planets populations.

The current complement of known L and T dwarfs allows some constraints to be placed on the substellar mass function (e.g. Chabrier 2003 and references therein; Allen et al. 2005; Metchev et al. 2008). However, if the brown dwarf mass function is to be accurately constrained, a significantly larger number of late T dwarfs will be extremely beneficial, since the T_{eff} distribution of T dwarfs in the <950 K range is particularly sensitive to mass function variations (e.g. fig. 5 of Burgasser 2004). Furthermore, ac-

curate constraints on the brown dwarf birth rate (i.e. their formation history) need the improved statistics that come with larger numbers of both L and T dwarfs.

The United Kingdom Infrared Telescope (UKIRT) Infrared Deep Sky Survey (UKIDSS; Lawrence et al. 2007) is a new infrared survey being conducted with the UKIRT Wide Field Camera (WFCAM; Casali et al. 2007). UKIDSS is a set of five sub-surveys, with three wide-field surveys – the Large Area Survey (LAS), the Galactic Cluster Survey (GCS) and the Galactic Plane Survey (GPS) – and two very deep surveys – the Deep Extragalactic Survey (DXS) and the Ultra-Deep Survey (UDS). The LAS is the largest of the wide-field surveys, and will cover 4000 deg^2 of sky in four filter bands, going several magnitudes deeper than 2MASS. UKIDSS began in 2005 May, and at the time of writing there have been four European Southern Observatory (ESO)-wide releases, including an Early Data Release (EDR) in 2006 February (Dye et al. 2006), and three subsequent main data releases: Data Release 1 (DR1) in 2006 July covering 190 deg^2 (Warren et al. 2007a), Data Release 2 (DR2) in 2007 March covering 280 deg^2 (including DR1; Warren et al. 2007c) and Data Release 3 (DR3) in 2007 December covering 900 deg^2 (including DR1 and DR2).

These data are providing unparalleled sensitivity to L and T dwarf populations, and our collaboration has begun a variety of UKIDSS-based searches for these objects. Here we focus on our search for late T dwarfs and potentially new record breaking low- T_{eff} objects. Previous LAS T dwarfs have been presented by Kendall et al. (2007), Lodieu et al. (2007a), Warren et al. (2007b) and Chiu et al. (2008), who have discovered a total of 13 spectroscopically confirmed LAS T dwarfs from the EDR and DR1. This included the first T8.5 dwarf ULAS J0034–0052 (Warren et al. 2007b).

Here we report the discovery of 15 new LAS T dwarfs discovered in DR1, DR2 and some of DR3. Section 2 summarizes our selection criteria for identifying candidate T dwarfs as well as possible 400–700 K objects. Section 3 describes the follow-up photometry we have obtained to identify spurious objects amongst these candidates, and Section 4 presents our spectroscopic follow-up and confirmation of the 15 new T dwarfs. Section 5 discusses the spectral morphology and colour of the new T dwarfs and how these could relate to their physical properties, and Section 6 presents updated constraints on the size of the LAS T dwarf population, compared to theoretical predictions. Section 7 discusses some future work and gives our conclusions.

2 IDENTIFYING T DWARF CANDIDATES

In this section we describe our photometric search for T dwarfs and cooler 400–700 K objects (potential Y dwarfs). We will focus this description on our searches of DR1 and DR2, since our follow-up of candidates from these data releases has a reasonably

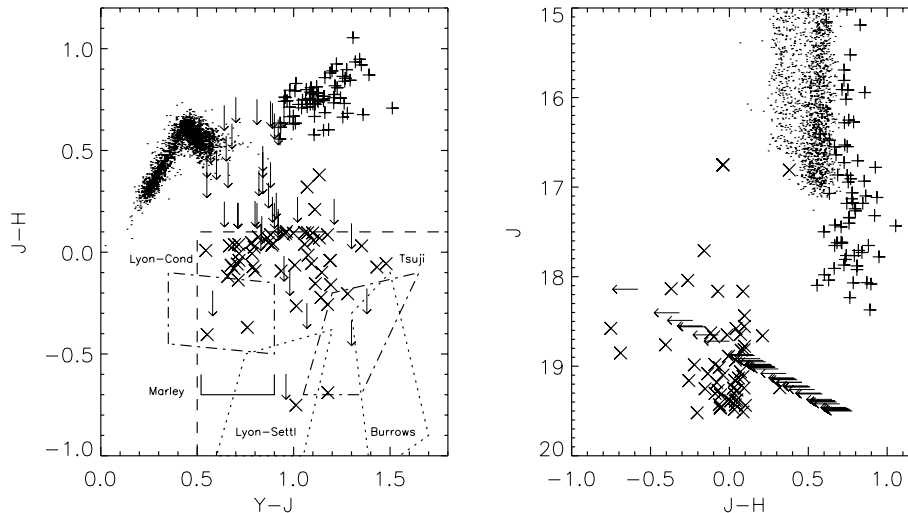


Figure 1. A $J - H$ against $Y - J$ two-colour diagram and a J against $J - H$ colour magnitude diagram showing candidate late T and Y dwarfs from DR1 and DR2. $YJH(K)$ candidates are shown as crosses, and YJ candidates as upper limit arrows. An illustrative L dwarf candidate sample is shown by plus signs. Our YJH candidate selection box is shown with a dashed line, and contains theoretical model predicted colours for $T_{\text{eff}} = 400\text{--}700$ K dwarfs from: the cloud-free Lyon-Cond models (Allard et al. 2001; Baraffe et al. 2003); the more recent Lyon-Settl models (Allard et al., in preparation); the AMES models (e.g. Marley et al. 2002; Saumon et al. 2003); the Tucson models (e.g. Burrows et al. 2006) and the Tsuji models (Tsuji et al. 2004).

well-constrained level of completion, and issues such as contamination amongst the candidates will be addressed more usefully. However, the process of T dwarf identification is ongoing with DR3, using these same techniques. Note also that some EDR/DR1 results have previously been published (Kendall et al. 2007; Lodieu et al. 2007a; Warren et al. 2007b), but for clarity we here describe our search of DR1 and DR2 as a whole.

We base our search on the current knowledge of $izJHK$ properties of known objects previously discovered in 2MASS and SDSS, as well as on colour trends suggested by the latest theoretical atmosphere models for T_{eff} ranges below those that are well probed by previous surveys. We also make use of LAS magnitudes measured using the new Y filter ($0.97\text{--}1.07\ \mu\text{m}$), which was specifically designed and installed in WFCAM to ease the selection and separation of high-redshift quasars and cool brown dwarfs (Warren & Hewett 2002).

2MASS T dwarfs have neutral to blue near-infrared colours with decreasing T_{eff} (Burgasser et al. 2002), and a fairly uniform $Y - J \sim 1$ (from synthesized colours; Hewett et al. 2006). Late T dwarfs are clearly well separated from redder L dwarfs by their $J - H$ colour (although there is some overlap for early T dwarfs and more generally LT transition objects e.g. Leggett et al. 2000b; Folkes et al. 2007), and from earlier objects by, in general, both $J - H$ and $Y - J$ colour (see Fig. 1). The model predictions suggest that the near-infrared colours will remain blue ($J - H < 0.0$, $J - K < 0.0$) for $400\text{--}700$ K. However, while the models uniformly predict that the $400\text{--}700$ K dwarf colour sequence should form an extension of the known T dwarfs, they differ somewhat on their predicted $Y - J$ colour trends. The cloud-free Cond models (Allard et al. 2001; Baraffe et al. 2003), the more recent Settl models (Allard et al., in preparation) and the Marley et al. (2002) models all suggest a blue $Y - J$ colour trend, while the Burrows et al. (2003) and Tsuji, Nakajima & Tanagisawa (2004) models suggest a red $Y - J$ colour trend for this T_{eff} regime.

In addition, T dwarfs found in SDSS have been selected by their very red ($i - z \geq 2.2$) optical colours, and/or extremely red optical-to-infrared colours ($z - J \geq 2.5$; note that here and hereafter i and z

are AB magnitudes whereas J is on the Vega system), the latter being a particularly good indicator of T_{eff} for early-mid T dwarfs (Knapp et al. 2004). The model predictions suggest that these extreme optical and optical-to-infrared colours should continue to be strong indicators of low T_{eff} in the $400\text{--}700$ K regime. A combination of $YJHK$ photometry from the LAS and deep optical constraints from SDSS thus offer an extremely powerful tool to identify samples of mid-late T dwarfs and even cooler objects to photometric depths several magnitudes deeper than previous wide-field surveys.

2.1 Initial sample selection

Our search methodology was to mine (via the WFCAM Science Archive; Hambly et al. 2008) the LAS for objects with $YJHK$ photometry consistent with known T dwarfs or with the expected colours of $400\text{--}700$ K objects using the models as a guide, and then cross-match with SDSS (where possible) to obtain optical-to-infrared constraints. Here we describe three sets of search criteria that probe to different depths in DR1 and DR2, requiring coverage in all four $YJHK$ bands, but relying on source detection in different numbers of bands.

Our first search method required $YJHK$ detection with $Y - J \geq 0.8$ and $J - H \leq 0.4$ (to separate T dwarfs from L dwarfs). This method is limited by the K band for mid-late T dwarfs, does not probe the full range of $Y - J$ colour for potential $400\text{--}700$ K objects, and is thus better at finding brighter early T dwarfs which can have redder $H - K$ colour. We also cross-matched objects with SDSS, requiring a detection with $i - z \geq 2.2$ and $z - J \geq 2.5$. While we also performed searches requiring optical non-detection, we postpone analysis of these candidates to a future publication, and here present the one new object identified with a SDSS detection: ULAS J115759.04+092200.7 (see Table 1).

Our second search method required YJH LAS detection and a K non-detection, and probed the colour space shown in Fig. 1, including objects with $J - H \leq 0.1$ and $Y - J \geq 0.5$. This search is H band limited for objects with blue $J - H$, but fully probes the range of $400\text{--}700$ K colour space suggested by the models.

Table 1. Newly discovered UKIDSS T dwarfs. The table lists the coordinates, the UKIDSS LAS data base release in which objects were found and the bands that were used to make the searches in which the objects were identified. All objects have SDSS coverage, although only one is detected in SDSS. The table contains the newly confirmed T dwarfs as well as (at the bottom) three that we rule out with spectroscopy.

Name ^a	Data base	NIR band detections	SDSS band detections
ULAS J022200.43-002410.5	DR1	<i>YJH</i>	–
ULAS J082327.46 + 002424.4	DR3	<i>YJHK</i>	–
ULAS J083756.19-004156.0	DR1	<i>YJH</i>	–
ULAS J085910.69 + 101017.1	DR3	<i>YJHK</i>	–
ULAS J093829.28-001112.6	DR3	<i>YJH</i>	–
ULAS J093951.04 + 001653.6	DR3	<i>YJH</i>	–
ULAS J095829.86-003932.0	DR1	<i>YJ</i>	–
ULAS J115038.79 + 094942.9	DR2	<i>YJH</i>	–
ULAS J115759.04 + 092200.7	DR2	<i>YJHK</i>	<i>i, z</i>
ULAS J130303.54 + 001627.7	DR1	<i>YJ</i>	–
ULAS J131508.42 + 082627.4	DR2	<i>YJH</i>	–
ULAS J150135.33 + 082215.2	DR2	<i>YJ</i>	–
ULAS J150547.89 + 070316.6	DR2	<i>YJ</i>	–
ULAS J154427.34 + 081926.6	DR2	<i>YJ</i>	–
ULAS J154701.84 + 005320.3	DR2	<i>YJH</i>	–
ULAS J003925.90 + 000257.7	DR1	<i>YJH</i>	–
ULAS J130150.35 + 002314.8 ^b	EDR	<i>YJH</i>	–
ULAS J224355.03-004618.5	DR1	<i>YJH</i>	–

^aHere the source names include full coordinates. In subsequent tables/figures the source names are truncated.

^bFirst reported as a T dwarf candidate by Kendall et al. (2007).

Candidates were cross-matched with SDSS and rejected if found to be optical detections with either $i - z < 2.2$ or $z - J < 2.5$, or found to have no SDSS coverage. This search produced a sample of 33 candidates.

Our third search method required *YJ* LAS detection and *HK* non-detection, with $Y - J \geq 0.5$. For objects with blue $J - H$ this search is J band or Y band limited for $Y - J \leq 0.8$ and $Y - J \geq 0.8$, respectively, and probes to a greater depth than method 2. SDSS cross-matching constraints were imposed as before, and resulted in a sample of 45 candidates.

In addition we used our second search method to search the LAS sky outside the SDSS DR6 footprint, substituting our SDSS optical constraints for shallower Schmidt plate I -band coverage from the SuperCOSMOS sky survey. This search identified 24 candidates.

Fig. 1 shows the $J - H$, $Y - J$ two-colour diagram and the J against $J - H$ colour–magnitude diagram for the T dwarf and $T_{\text{eff}} = 400\text{--}700\text{ K}$ candidates from DR1 and DR2. Candidates are either crosses (where Y -, J - and H -band detections were available) or arrows (where H was a non-detection). A sample of L dwarf candidates (plus signs; $LAS\ Y - J > 0.9, J - H > 0.5, J - K > 1.2$, and $SDSS\ z < 20.8$) is also shown for comparison (some spectroscopically confirmed L dwarfs from this sample will be reported in a separate paper), as is a sample of typical brighter sources from the LAS (points). These brighter sources were selected from a 1° radius area of DR2 sky at high Galactic latitude, and have *YJHK* magnitude uncertainties less than 0.03 mag and a Sloan counterpart. The L dwarf candidates are being followed up, but we will not discuss them further here, showing them purely for comparison. Our *YJH* selection box ($Y - J > 0.5, J - H < 0.1$) is indicated with a dashed line, and contains overplotted boxes (dotted and dot–dashed lines)

that illustrate the range of model predictions for $T_{\text{eff}} = 400\text{--}700\text{ K}$ (see figure caption).

Candidates from our DR1–3 searches that have been confirmed as T dwarfs via spectroscopy (see Section 4) are shown in Table 1, which summarizes the data base release in which they were first found, as well as the bands that were used to make the searches. All of our new T dwarfs are covered by SDSS DR6 sky, although two previously confirmed candidates (Lodieu et al. 2007a) are outside the SDSS DR6 footprint. Fig. 2 presents finding charts for the 15 new T dwarfs.

3 FOLLOW-UP PHOTOMETRY

Photometric contamination amongst our candidates has several causes. In general, photometry near the survey limits will have significant uncertainties due to low signal-to-noise ratio and/or survey image defects (see Dye et al. 2006), and in certain circumstances normal stars can have their colours scattered to the blue. Scattered late M dwarfs with $J > 18$ will not always be ruled out via SDSS non-detection if their $i - J = 3\text{--}4$ (the 5σ SDSS i -band limit is ~ 22). Furthermore, if LAS images in different bands are measured on different nights, variable sources can yield extremely blue survey colours, and fast moving Solar system objects can appear as detections at Y and J while being undetected (at that position) in H and K . Galaxies can also have unusual colours that could contaminate our selections.

We used deeper follow-up J - and H -band photometry to identify such contamination, remeasuring the $J - H$ colour at a higher signal-to-noise ratio and identifying any extended sources. We also obtained deeper Y -, K - and z -band photometry of a number of our best candidates to provide a more complete range of colours with which to assess candidate properties. We used a variety of facilities to obtain our infrared and optical follow-up photometry, and we summarize these measurements for confirmed T dwarfs in Table 2. In general this table presents photometry for the newly discovered T dwarfs, but also includes additional z -band measurements for two previously reported LAS T dwarfs from Lodieu et al. (2007a).

3.1 Near-infrared photometry

Near-infrared follow-up photometry was obtained with three facilities. We used WFCAM and the UKIRT Fast-Track Imager (UFTI; Roche et al. 2003) on UKIRT, both of which employ the Mauna Kea Observatories (MKO) J , H and K filters (Tokunaga, Simons & Vacca 2002), as well as the UKIDSS Y filter (Hewett et al. 2006). We also used the Long-slit Infrared Imaging Spectrograph (LIRIS; Manchado et al. 1998) instrument on the William Herschel Telescope on La Palma in the Canaries, which uses MKO J and H filters, a K_s filter and a z_{LIRIS} filter that is quite similar (although slightly narrower band; $1.00\text{--}1.07\ \mu\text{m}$) to WFCAM Y . It also has a narrow-band methane filter (CH_4 ; $1.64\text{--}1.74\ \mu\text{m}$) that we used to measure one of the new T dwarfs presented here.

Observations comprised a series of jittered (by a few arcsec) image sets, as well as (for WFCAM observations) subsets of microstepped images that improve the pixel sampling during processing. Individual exposure times ranged from 10 to 216 s, and a summary of the different combinations of microstep, jitter (dither), repeat, individual exposure time and total exposure times is given in Table 2. All observations were made during photometric conditions with good to reasonable seeing (0.6–0.8 arcsec). The data was

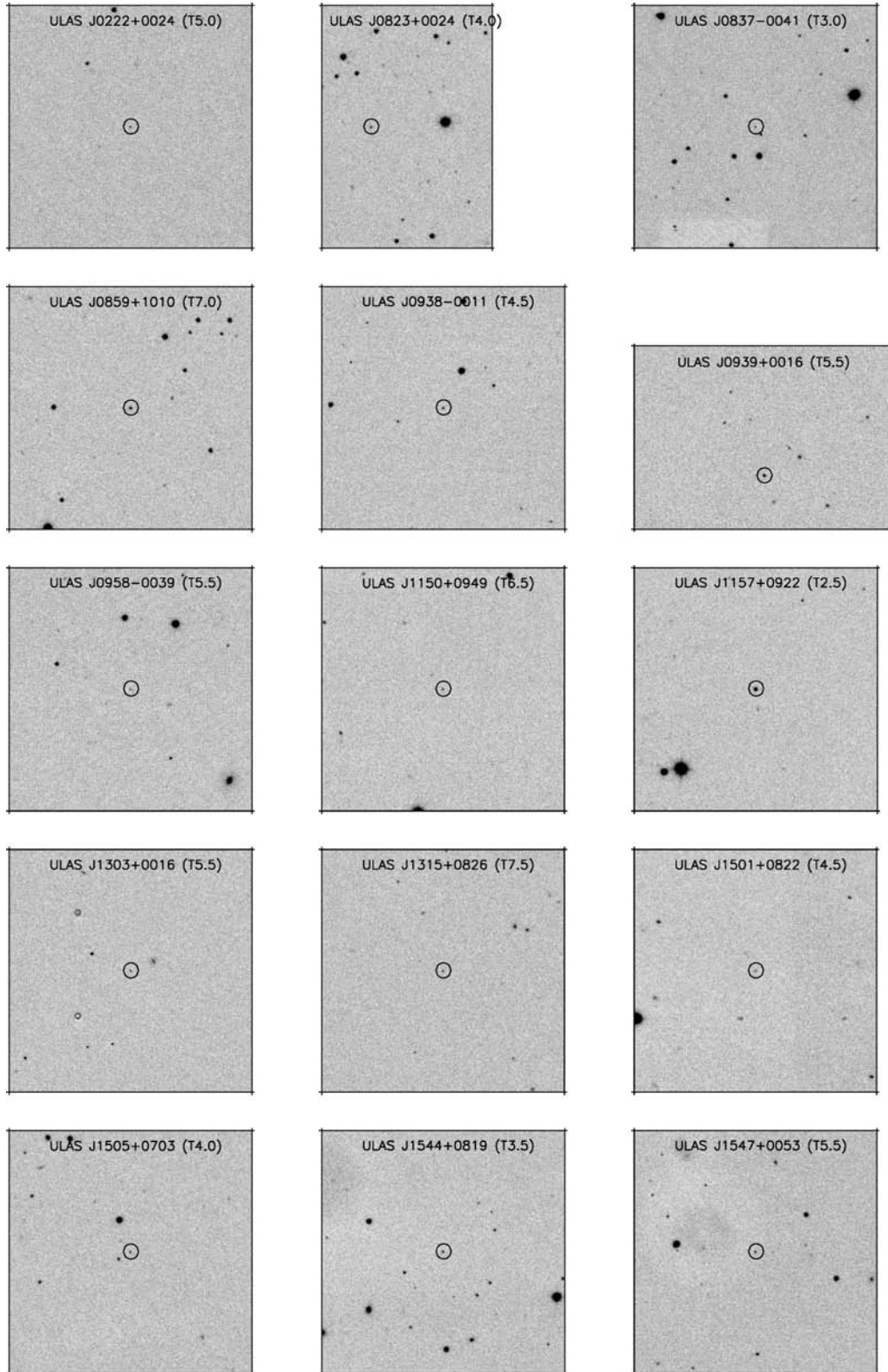


Figure 2. Finding charts for the 15 new T dwarfs discovered in the UKIDSS LAS and presented in this paper. Charts are *J*-band images of generally 2 arcmin on a side (unless constrained by the edge of a UKIDSS frame) with north up and east left. Indicated spectral types are infrared types derived here.

dark subtracted, flat-fielded and mosaiced using standard ORAC-DR routines for the UFTI data, LIRIS-DR routines for the LIRIS data and the Cambridge Astronomical Survey Unit's Vista data-flow system (Irwin et al. 2004) for the WFCAM observations. Photom-

etry was then performed using typical aperture sizes of ~ 2 -arcsec diameter.

The UFTI observations were calibrated using UKIRT Faint Standards, so the photometric system was thus identical to the

Table 2. Follow-up near-infrared and optical photometric observations.

Name	Instrument/ telescope	Filter	UT date	t_{int} ($m = \text{microsteps}, j = \text{jitters}, r = \text{repeats}$) ^a
ULAS J0222–0024	UFTI/UKIRT	<i>J</i>	2007 July 24	300 s ($j = 5, t_{\text{exp}} = 60$ s)
		<i>H</i>		1800 s ($j = 5, r = 6, t_{\text{exp}} = 60$ s)
		<i>K</i>	2007 July 28	1590 s ($j = 5, r = 6, t_{\text{exp}} = 53$ s)
		<i>Y</i>		600 s ($j = 5, t_{\text{exp}} = 120$ s)
ULAS J0823+0024	EMMI/NTT	ζ EMMI	2007 November 17	2400 s ($r = 4, t_{\text{exp}} = 600$ s)
	EMMI/NTT	ζ EMMI	2007 November 17	900 s ($r = 2, t_{\text{exp}} = 450$ s)
ULAS J0837–0041	WFCAM/UKIRT	<i>J</i>	2007 May 9	320 s ($m = 4, j = 2, r = 4, t_{\text{exp}} = 10$ s)
		<i>H</i>		800 s ($m = 4, j = 5, r = 4, t_{\text{exp}} = 10$ s)
ULAS J0859+1010	LIRIS/WHT	ζ EMMI	2008 January 30	2400 s ($r = 4, t_{\text{exp}} = 600$ s)
		<i>H</i>	2007 December 16	504 s ($j = 9, r = 14, t_{\text{exp}} = 4$ s)
		<i>CH₄l</i>	2007 December 16	450 s ($j = 9, r = 5, t_{\text{exp}} = 10$ s)
ULAS J0938–0011	EMMI/NTT	ζ EMMI	2007 November 17	600 s ($r = 1, t_{\text{exp}} = 600$ s)
	EMMI/NTT	ζ EMMI	2008 January 29	1800 s ($r = 3, t_{\text{exp}} = 600$ s)
ULAS J0939+0016	EMMI/NTT	ζ EMMI	2008 January 31	900 s ($r = 2, t_{\text{exp}} = 450$ s)
ULAS J0958–0039	LIRIS/WHT	<i>J</i>	2007 March 1	400 s ($j = 5, r = 2, t_{\text{exp}} = 40$ s)
		<i>H</i>		600 s ($j = 5, r = 6, t_{\text{exp}} = 20$ s)
		<i>K_s</i>		800 s ($j = 5, r = 8, t_{\text{exp}} = 20$ s)
		ζ EMMI	2008 January 30	2400 s ($r = 4, t_{\text{exp}} = 600$ s)
		<i>J</i>	2007 March 2	200 s ($j = 5, t_{\text{exp}} = 40$ s)
ULAS J1150+0949	LIRIS/WHT	<i>H</i>		1200 s ($j = 5, r = 12, t_{\text{exp}} = 20$ s)
		<i>K_s</i>		1800 s ($j = 5, r = 19, t_{\text{exp}} = 20$ s)
		<i>Y</i>		1200 s ($j = 5, r = 6, t_{\text{exp}} = 40$ s)
		ζ EMMI	2008 January 30	2400 s ($r = 4, t_{\text{exp}} = 600$ s)
ULAS J1157+0922 ^b	LIRIS/WHT	<i>J</i>	2007 March 3	200 s ($j = 5, t_{\text{exp}} = 40$ s)
<i>H</i>			1200 s ($j = 5, r = 12, t_{\text{exp}} = 20$ s)	
<i>K_s</i>			1800 s ($j = 5, r = 18, t_{\text{exp}} = 20$ s)	
ULAS J1315+0826	LIRIS/WHT	<i>J</i>	2007 March 2	200 s ($j = 5, t_{\text{exp}} = 40$ s)
		<i>H</i>		400 s ($j = 5, r = 4, t_{\text{exp}} = 20$ s)
		<i>K_s</i>		1000 s ($j = 5, r = 10, t_{\text{exp}} = 20$ s)
		<i>Y</i>		1000 s ($j = 5, r = 5, t_{\text{exp}} = 40$ s)
		ζ EMMI	2008 January 31	2400 s ($r = 4, t_{\text{exp}} = 600$ s)
ULAS J1501+0822	LIRIS/WHT	<i>J</i>	2007 March 2	200 s ($j = 5, t_{\text{exp}} = 40$ s)
		<i>H</i>		400 s ($j = 5, r = 4, t_{\text{exp}} = 20$ s)
		<i>K_s</i>		800 s ($j = 5, r = 8, t_{\text{exp}} = 20$ s)
ULAS J1505+0703	UFTI/UKIRT	<i>J</i>	2007 July 23	540 s ($j = 9, t_{\text{exp}} = 60$ s)
		<i>H</i>		3240 s ($j = 9, r = 6, t_{\text{exp}} = 60$ s)
		<i>K</i>		3240 s ($j = 9, r = 6, t_{\text{exp}} = 60$ s)
		<i>Y</i>		2160 s ($j = 5, r = 2, t_{\text{exp}} = 216$ s)
ULAS J1544+0819	UFTI/UKIRT	<i>J</i>	2007 July 15	300 s ($j = 5, t_{\text{exp}} = 60$ s)
		<i>H</i>		1800 s ($j = 5, r = 6, t_{\text{exp}} = 60$ s)
		<i>K</i>		1800 s ($j = 5, r = 6, t_{\text{exp}} = 60$ s)
		<i>Y</i>		1080 s ($j = 5, t_{\text{exp}} = 216$ s)
ULAS J1547+0053	LIRIS/WHT	<i>J</i>	2007 March 2	200 s ($j = 5, t_{\text{exp}} = 40$ s)
		<i>H</i>		600 s ($j = 5, r = 6, t_{\text{exp}} = 20$ s)
		<i>K_s</i>		800 s ($j = 5, r = 8, t_{\text{exp}} = 20$ s)
		<i>Y</i>		800 s ($j = 5, r = 4, t_{\text{exp}} = 40$ s)
ULAS J0024+0022 ^c	EMMI/NTT	ζ EMMI	2007 November 16	2400 s ($r = 4, t_{\text{exp}} = 600$ s)
ULAS J0203–0102 ^c	EMMI/NTT	ζ EMMI	2007 November 17	1800 s ($r = 3, t_{\text{exp}} = 600$ s)

^aPhotometric observations consist of a combination of microsteps, jitters (or dithers) and repeats (see Dye et al. 2006 for terminology) of a single integration time (t_{exp}) that combine to a total integration time (t_{int}).^bNo photometric follow-up was made of this T dwarf.^cT dwarfs from Lodieu et al. (2007a).

WFCAM system (Leggett et al. 2006). The WFCAM magnitudes were obtained via flat-file access from the WFCAM Science Archive. The LIRIS *J*-, *H*- and *K_s*-band observations were calibrated using 2MASS stars as secondary standards where *J* and *H* magnitudes were converted on to the MKO system via transforms from Warren et al. (2007c). 2MASS uses the same *K_s* filter as LIRIS, so no 2MASS standard *K* conversion was

necessary when determining LIRIS *K_s* magnitudes for our candidates. LIRIS *CH₄l* photometry was calibrated by assuming that the average *H* – *CH₄l* colours of 2MASS secondary calibrators was zero (see also Kendall et al. 2007). The LIRIS *z* observations were calibrated using observations of A0 stars at similar airmass to our target observations, where $(z - J)_{A0} = 0$ was assumed.

In order for the T dwarf photometry to be in the same photometric system, we converted our LIRIS z and K_s measurements to MKO Y and K . Transforms were determined via synthetic colours derived from measured T dwarf spectra multiplied by the appropriate atmospheric and filter transmission profiles, following the methods of Hewett et al. (2006). We derived $Y - z_{\text{LIRIS}}$ and $K - K_s(\text{LIRIS})$ colours for the standard T dwarfs from B06 as well as for the T dwarfs used in Hewett et al. (2006), excepting objects that have been shown to be unresolved binaries (Burgasser et al. 2006a; Liu et al. 2006). The $Y - z_{\text{LIRIS}}$ colours show no trend with spectral type, and a conversion of $Y = z_{\text{LIRIS}} + (0.015 \pm 0.011)$ was determined. The $K - K_s(\text{WHT})$ colours display a tightly defined sequence monotonically increasing with spectral type such that $K = K_s(\text{WHT}) + (0.032 \times \text{ST}) - 0.01$, with a scatter of 0.01 mag (where $\text{ST} = 1, 2, 3, \dots$ for T1, T2, T3, ...).

3.2 Optical photometry

Optical z -band follow-up photometry was obtained with the European Southern Observatory (ESO) Multi-Mode Instrument (EMMI) on the New Technology Telescope on La Silla, Chile. A Bessel z -band filter was used (EMMI#611; z_{EMMI}) which has a short wavelength cut-off of 825 nm and is an open-ended filter, where the CCD sensitivity provides the longer wavelength cut-off. The conditions were clear, with seeing of ~ 1 arcsec. The EMMI data were reduced using standard IRAF routines including a bias and flat-field correction, as well as the removal of fringing effects. Multiple images of the same sky areas were then aligned and co-added. Aperture photometry was measured using ~ 1.5 -arcsec apertures, and we calibrated this photometry using Sloan sources (York et al. 2000) contained in the images as secondary standards. This method allowed us to derive image zero points with a typical accuracy of ± 0.05 mag. We transformed the Sloan AB photometry of our secondary standards into the EMMI system using the transformation of Warren et al. (2007b). We then derived z_{EMMI} (AB) photometry for the targets, and then transformed these into the Sloan AB magnitudes assuming that $z(\text{AB}) = z_{\text{EMMI}}(\text{AB}) + 0.2$ (Warren et al. 2007b). Our optical z -band photometry is thus all in the Sloan AB system.

3.3 Photometric results

We have been able to reject 61 of our 103 DR1 and DR2 candidates via follow-up photometry, since the $J - H$ colours were found to be ≥ 0.4 , and the candidates thus likely M or L dwarfs. A total of 23 DR1 and DR2 T dwarfs have been confirmed amongst the remaining candidates, including 11 of the 15 new T dwarfs reported here (four are from DR3), and 12 previously reported: one by Kendall et al. (2007), one by Warren et al. (2007b), eight by Lodieu et al. (2007a), one by Chiu et al. (2007) and one previously found in SDSS (Geballe et al. 2002). Near-infrared and optical photometry for all 15 newly discovered T dwarfs is shown in Table 3, and their spectroscopic confirmation is discussed in Section 4. One of the remaining candidates has follow-up photometric colours that suggest it is an additional T dwarf (but no spectrum has been obtained to date), and 18 candidates still await follow-up. Further discussion of the magnitude-limited completeness of our follow-up will be presented in Section 6.

4 SPECTROSCOPIC OBSERVATIONS

Spectroscopic follow-up observations were made at five different facilities, providing a variety of near-infrared spectral ranges and

sensitivities. Table 4 summarizes which facilities were used to observe the newly confirmed T dwarfs in this work (as well as three candidates that were ruled out by spectroscopy), and gives details on the wavelength range covered, the date of the observations and the total exposure times used. A description of these facilities and the reduction methods used is given in the next sections.

4.1 Gemini/GNIRS spectroscopy

The Gemini Near-Infrared Spectrograph (GNIRS; Elias et al. 2006) on Gemini South was used to make quick response observations, through programme GS-2007A-Q-15. GNIRS was used in cross-dispersed mode with the 321 mm^{-1} grism, the 1.0-arcsec slit and the short camera, to obtain 0.9–2.5 μm , $R \simeq 500$ (per resolution element) spectra. The targets were nodded 3 arcsec along the slit in an ABBA pattern using individual exposure times of 240 s. Calibrations were achieved using lamps in the on-telescope calibration unit. A0 and early F stars were observed as spectroscopic standards, either directly before or after the target observations, at an airmass that closely matched the mid-point airmass of the target, in order to remove the effects of telluric absorption. The observing conditions included some patchy cloud, seeing from 0.5 to 1.0 arcsec, and humidity ranging from 10 to 50 per cent.

Data reduction was initially implemented using tasks in the Gemini GNIRS IRAF¹ (Image Reduction and Analysis Facility) package. Files were prepared and corrected for offset bias using NSPREPARE and NVNOISE, and order separation achieved with NSCUT. Each order was then median stacked at the A and B positions, and a difference image obtained using GEMARITH. Flat-field correction was not necessary since variations across the 6-arcsec slit are less than 0.1 per cent, and any flat-field variations in the dispersion direction will subsequently be removed when dividing by the spectrum of a standard. S-distortion correction and wavelength calibration were performed interactively using the telluric star spectra and argon arc lamp spectra, with NSAPPWAVE, NSSDIST and NSWAVE. Further reduction was carried out using custom written IDL (Interactive Data Language) routines. Apertures (1.5-arcsec wide) were centred on the spectra at the A and B positions, and the sky residuals were fit (and subtracted) using a surface constructed via a series of least-squares linear fits across the slit (excluding pixels within the apertures), with one fit for each spatial pixel row. Spectra were then extracted by summing within the A and B position apertures and combining. The target spectra were flux calibrated on a relative scale using the telluric standard spectra (after appropriate interpolation across any hydrogen absorption lines) with an assumed blackbody function for $T_{\text{eff}} = 10000$ and 7000 K for A0 and early F tellurics (e.g. Masana, Jordi & Ribas 2006), respectively. The spectral orders were then trimmed of their noisiest portions, and the spectra normalized to unity at $1.27 \pm 0.005 \mu\text{m}$.

4.2 Gemini/NIRI spectroscopy

Gemini's Near-Infrared Camera and Spectrometer (NIRI; Hodapp et al. 2003) was used, on the Gemini North Telescope on Mauna Kea, Hawaii, through programme GN-2007B-Q-26. NIRI was used in the f/6 mode with a 0.75-arcsec slit, and with the J grism (312.61 mm^{-1}) and G0209 order sorting filter. This produced $R \sim 460$ spectra over

¹ IRAF is distributed by the National Optical Astronomy Observatories, which are operated by the Association of Universities for Research in Astronomy, Inc., under cooperative agreement with the National Science Foundation.

Table 3. T dwarf photometry and colours. Unless otherwise indicated, near-infrared photometry was measured on the MKO system. The last two T dwarfs are from Lodieu et al. (2007a), and here we present additional z -band measurements. Note that z photometry is on the AB system and all other photometry is on the Vega system.

Name	Y	J	H	K	z_{AB}	Y - J	J - H	H - K	$z_{AB} - J$
ULAS J0222-0024	19.87 ± 0.03	18.71 ± 0.02	19.02 ± 0.02	19.18 ± 0.03	22.50 ± 0.07 ^a	1.16 ± 0.04	-0.31 ± 0.03	-0.16 ± 0.04	3.79 ± 0.07
ULAS J0823+0024	19.93 ± 0.15 ^b	18.57 ± 0.05 ^b	18.96 ± 0.18 ^b	18.58 ± 0.23 ^b	22.80 ± 0.15	1.36 ± 0.16	-0.39 ± 0.19	0.38 ± 0.29	4.23 ± 0.16
ULAS J0837-0041	19.64 ± 0.03 ^b	18.52 ± 0.09	18.60 ± 0.11		22.18 ± 0.06	1.12 ± 0.09	-0.08 ± 0.14		3.66 ± 0.11
ULAS J0859+1010 ^c	19.00 ± 0.07 ^b	17.88 ± 0.06 ^b	18.58 ± 0.06	18.26 ± 0.15 ^b	21.53 ± 0.05	1.12 ± 0.09	-0.70 ± 0.08	0.32 ± 0.16	3.65 ± 0.08
ULAS J0938-0011	19.83 ± 0.12 ^b	18.53 ± 0.06 ^b	19.00 ± 0.19 ^b		22.27 ± 0.05	1.30 ± 0.13	-0.47 ± 0.20		3.74 ± 0.08
ULAS J0939+0016	19.20 ± 0.07 ^b	17.96 ± 0.03 ^b	18.41 ± 0.11 ^b		21.74 ± 0.05	1.24 ± 0.08	-0.45 ± 0.11		3.78 ± 0.06
ULAS J0958-0039	19.88 ± 0.15 ^b	18.95 ± 0.06	19.40 ± 0.10	19.68 ± 0.12 ^d	22.85 ± 0.09	0.93 ± 0.16	-0.45 ± 0.12	-0.28 ± 0.16	3.90 ± 0.10
ULAS J1150+0949	19.92 ± 0.08 ^e	18.68 ± 0.04	19.23 ± 0.06	19.06 ± 0.05 ^d	22.44 ± 0.10	1.24 ± 0.09	-0.55 ± 0.07	0.17 ± 0.08	3.76 ± 0.11
ULAS J1157+0922	17.94 ± 0.03 ^b	16.81 ± 0.01 ^b	16.43 ± 0.02 ^b	16.24 ± 0.04 ^b		1.13 ± 0.03	0.38 ± 0.02	0.19 ± 0.04	
ULAS J1303+0016	20.21 ± 0.17 ^b	19.02 ± 0.03	19.49 ± 0.09	20.10 ± 0.17 ^d		1.19 ± 0.17	-0.47 ± 0.09	-0.61 ± 0.19	
ULAS J1315+0826	20.00 ± 0.08 ^e	18.86 ± 0.04	19.50 ± 0.10	19.60 ± 0.12 ^d	22.82 ± 0.10	1.14 ± 0.09	-0.64 ± 0.11	-0.10 ± 0.16	3.96 ± 0.11
ULAS J1501+0822	19.70 ± 0.15 ^b	18.32 ± 0.02	18.30 ± 0.06	18.53 ± 0.10 ^d		1.38 ± 0.15	0.02 ± 0.06	-0.23 ± 0.12	
ULAS J1505+0703	20.32 ± 0.02	18.96 ± 0.03	19.10 ± 0.03	19.29 ± 0.03		1.36 ± 0.04	-0.14 ± 0.04	-0.19 ± 0.04	
ULAS J1544+0819	19.80 ± 0.05	18.53 ± 0.03	18.49 ± 0.03	18.73 ± 0.03		1.27 ± 0.06	0.04 ± 0.03	-0.24 ± 0.04	
ULAS J1547+0053	19.37 ± 0.06 ^e	18.32 ± 0.03	18.45 ± 0.07	18.21 ± 0.10 ^d		1.05 ± 0.07	-0.13 ± 0.08	0.24 ± 0.12	
ULAS J0024+0022 ^f					22.77 ± 0.10 ^g				4.61 ± 0.10
ULAS J0203-0102 ^f					22.11 ± 0.06 ^g				4.07 ± 0.06

^a z_{EMMI} converted into z_{spss} .

^b Photometry from the UKIDSS LAS.

^c Also has a measured $H - CH_4J$ colour of -1.05 ± 0.12 , typical of mid-late T dwarfs.

^d K_s (Liris) converted into K (MKO).

^e z_{Liris} converted into Y (MKO).

^f T dwarfs from Lodieu et al. (2007a).

Table 4. Spectroscopic observations. The table contains the new confirmed T dwarfs, as well as (at the bottom) three that we rule out with spectroscopy.

Name	Instrument/ telescope	Wavelength range	UT date	t_{int}
ULAS J0222–0024	NIRI/Gemini-N	1.05–1.41 μm	2007 September 2	960 s (4 \times 240 s)
ULAS J0823+0024	NIRI/Gemini-N	1.05–1.41 μm	2007 September 2	960 s (4 \times 240 s)
ULAS J0837–0041	NIRI/Gemini-N	1.05–1.41 μm	2007 October 5	960 s (4 \times 240 s)
ULAS J0859+1010	NIRI/Gemini-N	1.05–1.41 μm	2007 September 2	960 s (4 \times 240 s)
ULAS J0938–0011	NIRI/Gemini-N	1.05–1.41 μm	2007 September 2	960 s (4 \times 240 s)
ULAS J0939+0016	NIRI/Gemini-N	1.05–1.41 μm	2007 September 2	960 s (4 \times 240 s)
ULAS J0958–0039	GNIRS/Gemini-S	0.9–2.5 μm	2007 April 4	960 s (4 \times 240 s)
ULAS J1150+0949	GNIRS/Gemini-S	0.9–2.5 μm	2007 March 10	960 s (4 \times 240 s)
ULAS J1157+0922	NICS/TNG	0.9–2.5 μm	2007 April 9	1200 s (4 \times 300 s)
	UIST/UKIRT	1.4–2.5 μm	2007 June 27	5760 s (24 \times 240 s)
ULAS J1303+0016	GNIRS/Gemini-S	0.9–2.5 μm	2007 March 10	960 s (4 \times 240 s)
ULAS J1315+0826	GNIRS/Gemini-S	0.9–2.5 μm	2007 April 4	960 s (4 \times 240 s)
ULAS J1501+0822	IRCS/Subaru	1–1.6 μm	2007 July 1	2400 s (8 \times 300 s)
ULAS J1505+0703	NIRI/Gemini-N	1.05–1.41 μm	2007 August 22	1200 s (4 \times 300 s)
ULAS J1544+0819	NIRI/Gemini-N	1.05–1.41 μm	2007 September 4	960 s (4 \times 240 s)
ULAS J1547+0053	IRCS/Subaru	1–1.6 μm	2007 July 1	1920 s (8 \times 240 s)
ULAS J0039+0002	IRCS/Subaru	1–1.6 μm	2007 July 1	1920 s (8 \times 240 s)
ULAS J1301+0023	IRCS/Subaru	1–1.6 μm	2007 July 1	1920 s (8 \times 240 s)
ULAS J2243–0046	IRCS/Subaru	1–1.6 μm	2007 July 1	1920 s (8 \times 240 s)

1.05–1.41 μm . The targets were nodded 10 arcsec along the slit in an ABBA pattern, and calibrations were achieved using argon lamp observations (as with GNIRS), and F stars as telluric standards. The observing conditions were very similar to those of the GNIRS observations.

NIRI data were reduced using tasks in the Gemini NIRI IRAF package. NRESID was used to create bad pixel masks from the individual flat-field observations. Combined flat-fields were created with NSFLAT, and then bad-pixel removal and flat-fielding of the science data was achieved using NSREDUCE. Sky removal was then carried out by subtracting consecutive AB pairs with GEMARITH, and multiple spectra combined with NSSTACK. We also minimized any pattern noise in our data using a custom written Python script, and wavelength calibrated with NSWAVE and corrected for any S-distortion with NSSDIST and NSTRANSFORM. Spectra were then extracted and calibrated using the same methods and software as were used for our GNIRS observations.

4.3 Subaru/IRCS spectroscopy

We used the Infrared Camera Spectrograph (IRCS; Kobayashi et al. 2000) on the Subaru Telescope on Mauna Kea, Hawaii. IRCS was used with its camera in the 52 mas pixel^{−1} mode, and with the *JH* grism and a 0.6-arcsec slit. This resulted in $R \sim 100$ spectra over a wavelength range of 1.0–1.6 μm . The targets were nodded 7 arcsec along the slit in an ABBA pattern. Calibrations were achieved using an argon lamp, and F2–5 stars were observed as telluric standards. The observing conditions were clear with seeing of ~ 0.7 arcsec.

The IRCS data were reduced following the same reduction procedures as were used for our NIRI data, but using generic spectral reduction IRAF packages. The only practical difference was that S-distortion correction and wavelength calibration were done at the same time, using the TRANSFORM package. Arc observations were obtained several times throughout the night, and we performed wavelength calibration with the arc closest in time to each target observation. We estimate wavelength residuals (by intercomparing arcs) of ~ 20 Å which should not affect significantly our subsequent analysis.

4.4 UKIRT/UIST spectroscopy

One of the T dwarfs (ULAS J1157+0922) was observed at UKIRT using the UKIRT Imager Spectrometer (UIST; Ramsay Howat et al. 2004). The *HK* grism was used with the 4-pixel slit, giving a resolution $R = 550$. Individual exposure times on target were 240 s, and the target was nodded up and down the slit by 12 arcsec. The instrument calibration lamps were used to provide accurate flat-fielding and wavelength calibration. The F5V star HD 96218 was observed prior to the target to remove the effects of telluric absorption, and to provide an approximate flux calibration. Relative flux calibration was improved by scaling the spectra to the *H* and *K* magnitudes measured in the LAS, and finally we scaled the spectra at 1.6 μm to join on to our broader wavelength Telescope Nazionale Galileo (TNG) spectra (see next section).

4.5 TNG/NICS spectroscopy

We have also obtained a low-resolution ($R \sim 50$) near-infrared (0.9–2.5 μm) spectrum of ULAS J1157+0922 with the Near-Infrared Camera Spectrometer (NICS; Baffa et al. 2001) on the TNG. The observations were made in service mode by the TNG staff, with seeing in the 1.2–2.0 arcsec range. NICS is a multipurpose instrument equipped with an HgCdTe Hawaii 1024 \times 1024 detector with 0.25 arcsec pixel^{−1}, yielding a 4.2 \times 4.2 arcmin² field-of-view. We employed the Amici mode with a 1-arcsec slit, yielding a wavelength coverage of 0.9–2.5 μm . Four integrations of 300 s were taken for the target in an ABBA dither pattern. A and B spectra were averaged, differenced and the resulting image flat-fielded. A one-dimensional spectrum was then extracted with the IRAF task APSUM. A standard star (HIP 48971; A0) was observed immediately after the target at a similar airmass, and divided through the science target to correct for telluric absorption, before flux calibrating with a blackbody of the same T_{eff} as the A0 star. Because of the low resolution of the Amici mode, virtually all the Ar/Xe arc lines are blended and cannot be easily used for standard reduction procedures. For this reason, wavelength calibration was performed in a NICS-specific way, using a look-up table (of wavelength against

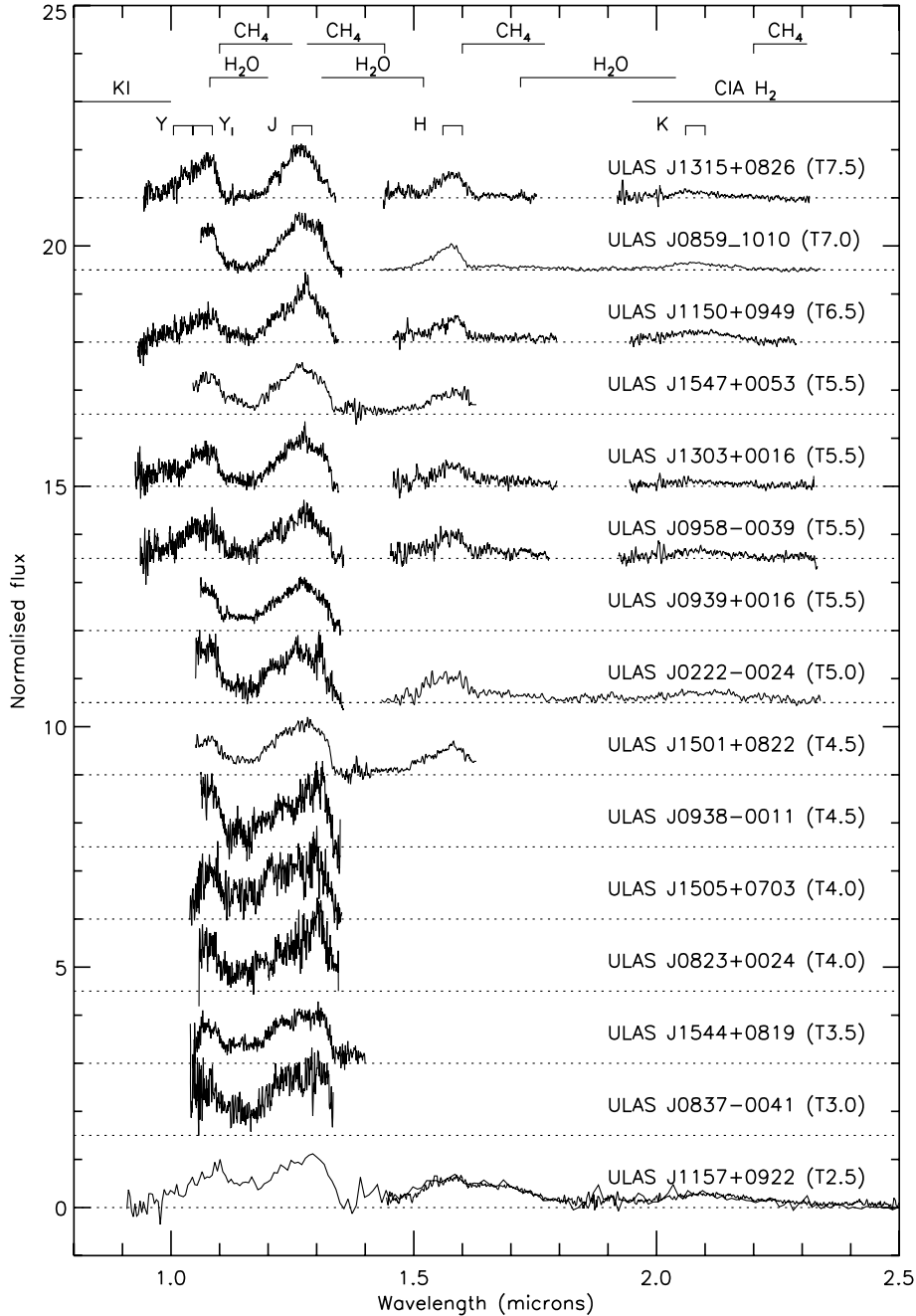


Figure 3. Spectra of the 15 new T dwarfs. The spectra are all normalized to unity at $1.27 \pm 0.005 \mu\text{m}$. Defining features of T dwarf spectra are indicated. Also shown are the Y , Y_1 , J , H and K bands which we use to calculate spectral peak ratios (see Section 5).

pixel) based on the instrument's theoretical dispersion from ray tracing. This first-pass wavelength calibration was then offset to best fit the observed spectra of the calibration sources. No attempt was made to correct the very modest level of slit curvature.

4.6 Spectral classification

Fig. 3 shows the spectra of the 15 new T dwarfs. For each spectrum we calculated all available near-infrared spectral indices from B06; $\text{H}_2\text{O} - J$, $\text{CH}_4 - J$, $\text{H}_2\text{O} - H$, $\text{CH}_4 - H$ and $\text{CH}_4 - K$. For the GNIRS and NICS spectra we were able to measure all five ratios. For the IRCS spectra we were able to measure $\text{H}_2\text{O} - J$, $\text{CH}_4 - J$ and

$\text{H}_2\text{O} - H$. The NIRS spectra allowed us to measure the $\text{H}_2\text{O} - J$ and $\text{CH}_4 - J$, and the UIST spectrum covered $\text{H}_2\text{O} - H$, $\text{CH}_4 - H$ and $\text{CH}_4 - K$. We also compared the data by eye to template spectra of T dwarfs defined by B06 as standard T4, T5, T6, T7 and T8 types. The results for the new T dwarfs are given in Table 5. Some scatter is present in the spectral indices given in Table 5 due to low signal-to-noise ratio. Consequently, the direct comparison with templates has been given more weight than the spectral indices in the assignment of spectral types, and the adopted uncertainty in Table 5 reflects the range in type implied by this comparison. Note also that in the case of one object (ULAS J1150+0949), the well measured $\text{H}_2\text{O} - H$ spectral ratio indicates a significantly earlier

Table 5. Spectral types derived from indices and by comparison with T dwarf templates (following B06).

Name	H ₂ O – <i>J</i>	CH ₄ – <i>J</i>	H ₂ O – <i>H</i>	CH ₄ – <i>H</i>	CH ₄ – <i>K</i>	Template	Adopted	Distance ^a (pc)
ULAS J0222–0024	0.272 (T5)	0.368 (T5.5)	0.358 (T5)	0.409 (T5)	0.587 (T2)	T5	T5 ± 0.5	55–78
ULAS J0823+0024	0.390 (T3)	0.696 (T1)				T4 ± 1	T4 ± 1	55–78
ULAS J0837–0041	0.419 (T3)	0.660 (T2)				T3	T3 ± 1	54–76
ULAS J0859+1010	0.058 (T8)	0.266 (T7)	0.219 (T7)	0.187 (T7)	0.136 (T6)	T7	T7 ± 0.5	26–36
ULAS J0938–0011	0.190 (T6)	0.484 (T4)				T4.5	T4.5 ± 1	53–75
ULAS J0939+0016	0.288 (T5)	0.366 (T5)				T5–6	T5.5 ± 1	37–52
ULAS J0958–0039	0.125 (T6.5)	0.341 (T5.5)	0.391 (T4)	0.402 (T5)	0.130 (T6.5)	T5.5 ± 1	T5.5 ± 1	58–82
ULAS J1150+0949	0.087 (T7)	0.302 (T6.5)	0.455 (T3)	0.230 (T6.5)	0.032 (≥T7)	T6–7	T6.5p ± 0.5	42–60
ULAS J1157+0922	0.428 (T3)	0.544 (T3)	0.453 (T3)	0.772 (T3)	0.557 (T2)	T2	T2.5 ± 0.5	24–34
ULAS J1303+0016	0.105 (T7)	0.324 (T6)	0.332 (T5.5)	0.367 (T5.5)	0.025 (≥T7)	T5–6	T5.5 ± 0.5	60–85
ULAS J1315+0826	0.034 (T8)	0.181 (T8)	0.227 (T7)	0.121 (T8)	0.080 (>T7)	T8	T7.5 ± 0.5	34–48
ULAS J1501+0822	0.290 (T5)	0.418 (T5)	0.411 (T4)			T4–5	T4.5 ± 0.5	48–68
ULAS J1505+0703	0.349 (T4)	0.572 (T2.5)				T4 ± 1	T4 ± 1	66–93
ULAS J1544+0819	0.411 (T3)	0.520 (T3.5)				T3.5	T3.5 ± 1	55–77
ULAS J1547+0053	0.217 (T5)	0.363 (T5)	0.331 (T5)			T5–6	T5.5 ± 0.5	44–61

^aAssumes single objects.

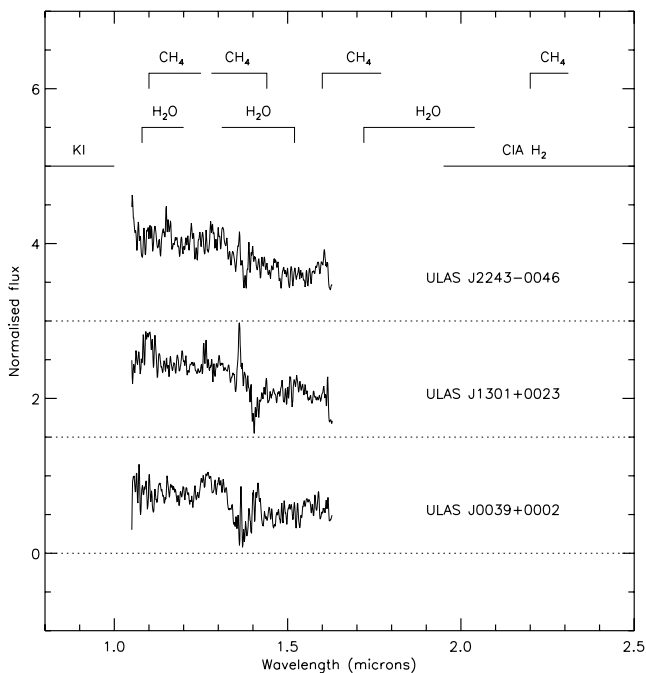


Figure 4. Spectra of the three T dwarf candidates ruled out with spectroscopy. The absorption features that we expect to define T dwarf spectra are indicated, and are clearly not present in these spectra.

spectral type (T3) than all the other ratios for this object (T6–7), and we have thus typed it as T6.5p. For ULAS J0222–0024 the CH₄ – *K* index appears discrepant, but the signal-to-noise for this spectral region is poor and we cannot at this stage confirm this ratio. Table 5 also presents distance estimates for the T dwarfs based on their spectral type and *J*-band brightness, using the M_J spectral-type relation (excluding known and possible binaries) of Liu et al. (2006), and allowing for the rms scatter in this relation.

Fig. 4 shows the Subaru spectra of the three candidates T dwarfs that we rule out with spectroscopy. Clearly none of these objects show the strong H₂O and CH₄ absorption at 1.1–1.2 and 1.3–1.5 μm that sculpts the *J*-band and *H*-band peaks characteristic of T dwarfs. After allowing for some residual telluric noise at ~1.4 μm,

the spectrum of ULAS J2243–0046 appears to have the form of a blue continuum. The other two sources show evidence of H₂O absorption at 1.3–1.4 μm, and appear to be M dwarfs. The LAS *YJ* and *HK* photometry used to select these candidates was taken on two separated nights, and variability might explain how some M dwarfs can appear to have blue *J* – *H* colours. ULAS J1301+0023 also showed some evidence for possible methane absorption (at the ~1–2σ level) via narrow-band CH₄*s*- and CH₄*l*-band photometry (Kendall et al. 2007). Our spectrum of this object does not cover the full wavelength range of these filters (1.53–1.63 and 1.64–1.74 μm, respectively), so we cannot rule out an intrinsically blue methane (CH₄*s* – CH₄*l*) colour. However, it may simply be that the relatively low signal-to-noise ratio of the narrow-band photometry led directly to the measurement of a blue colour.

5 T DWARF PROPERTIES

We now consider the overall spectral morphology of the T dwarfs using both their spectra and their photometric properties. We measured the relative brightness of the *Y*-, *J*-, *H*- and *K*-band spectral peaks by summing flux in several bands. In general we used the bands defined by Burgasser et al. (2006c), to which we also add an additional *Y* band at a slightly longer wavelength (which we refer to as *Y*_l). Our *Y*-, *Y*_l-, *J*-, *H*- and *K*-band spectral peaks cover the 1.005–1.045, 1.045–1.085, 1.25–1.29, 1.56–1.60 and 2.06–2.10 μm wavelength ranges, respectively, and are indicated in Fig. 5. Table 6 shows the integrated flux peak ratios for the 15 new T dwarfs. We were able to measure the *Y*_l/*J* ratio for all our T dwarf spectra, while the short wavelength cut-off in the spectral coverage of several of the T dwarfs precludes the measurement of the *YJ* ratio.

To assess how the spectral morphology of the T dwarfs may depend on their physical properties, we compare our observed properties with the predictions of model atmospheres. As a primary comparison we use the BT–Settl models (which combine with structure models to give the Lyon–Settl models shown in Fig. 1), generated with version 15.3 of the general-purpose stellar atmosphere code PHOENIX (Hauschildt & Baron 1999). These models use a set-up that currently gives the best BT–Settl fits to observed spectra of M, L and T dwarfs, updating the microphysics used in the GAIA model grid (Kucinskis et al. 2005, 2006). For a summary of the important input physics of these models, see Warren et al. (2007b). Note that

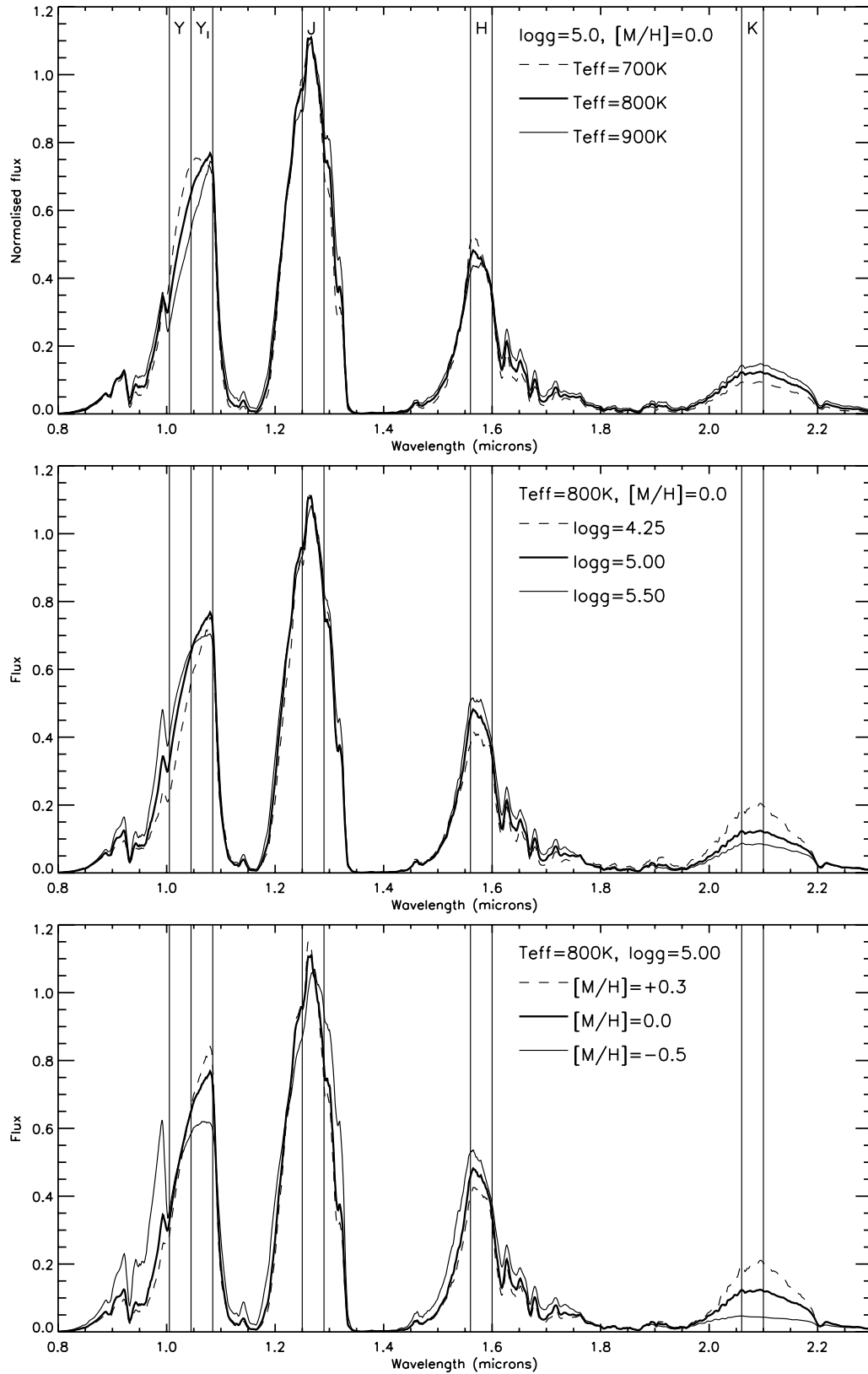


Figure 5. Model BT–Settl *T* dwarf spectra showing theoretical T_{eff} , $\log g$ and $[M/H]$ variations.

Burgasser et al. (2006c) and Leggett et al. (2007) have also examined these effects in the spectral models of Burrows, Sudarsky & Hubeny (2006, Tucson models) and Marley et al. (in preparation, AMES models), and while the different model trends in spectral

morphology are in broad agreement, we highlight any differences between these model sets and the BT–Settl models.

Fig. 5 demonstrates how the BT–Settl model spectra change with T_{eff} , gravity and metallicity. Our baseline properties in this figure

Table 6. Ratios of spectral peaks.

Name	SpT	Y/J	Y_1/J	H/J	K/J	K/H	Unusual property?
ULAS J0222–0024	T5.0	–	0.997	–	–	0.376	Noisy – possibly unusual metallicity
ULAS J0823+0024	T4.0	–	0.892	–	–	–	Normal
ULAS J0837–0041	T3.0	–	0.833	–	–	–	Normal
ULAS J0859+1010	T7.0	–	0.814	–	–	0.325	Normal
ULAS J0938–0011	T4.5	–	1.195	–	–	–	Noisy – possibly unusual metallicity
ULAS J0939+0016	T5.5	–	0.918	–	–	–	Normal
ULAS J0958–0039	T5.5	0.488	0.708	0.521	0.182	0.349	Noisy – possibly low T_{eff} or unusual metallicity
ULAS J1150+0949	T6.5	0.299	0.467	0.428	0.199	0.465	Low gravity ^a
ULAS J1157+0922	T2.5	0.401	0.467	0.652	0.291	0.446	Normal
ULAS J1303+0016	T5.5	0.416	0.738	0.449	0.110	0.245	High gravity
ULAS J1315+0826	T7.5	0.436	0.723	0.472	0.122	0.258	Normal
ULAS J1501+0822	T4.5	–	0.658	0.526	–	–	Normal
ULAS J1505+0703	T4.0	–	0.710	–	–	–	Normal
ULAS J1544+0819	T3.5	–	0.638	–	–	–	Normal
ULAS J1547+0053	T5.5	–	0.739	0.437	–	–	Low gravity ^b

^aPossibly high [M/H] as well.

^bFrom photometric colour only.

are $T_{\text{eff}} = 800$ K, $\log g = 5.0$, $[M/H] = 0.0$ and spectral variations for ± 100 K, $^{+0.5}_{-0.75}$ and $^{+0.3}_{-0.5}$ dex in T_{eff} , $\log g$ and $[M/H]$, respectively, are shown. The spectra have been normalized to unity at 1.27 ± 0.005 μm . As has been noted previously for the Tucson and AMES models, T_{eff} variations are significant in the wings of the H -band peak and in the peak of the K band. The BT–Settl models also suggest that the Y -band peak has some T_{eff} sensitivity, with increasing and decreasing T_{eff} suppressing and enhancing the Y -band flux (with respect to the J -band peak), respectively. By comparison the Tucson models also exhibit some Y -band variation with T_{eff} , but in the opposite sense to that of the BT–Settl models, and the AMES models show little variation with T_{eff} (Leggett et al. 2007). Gravity has a significant effect on the model K -band peak, with higher $\log g$ causing K -band suppression and lower $\log g$ enhancing the K -band flux. Some observational evidence may also support this trend, as for example, S Ori 70 (a possible T5.5 member of the ~ 3 Myr σ Orionis cluster; Zapatero-Osorio et al. 2008) and PLZ J93 (a possible T3–5 member of the Pleiades open cluster; Casewell et al. 2007) both show a strong K -band enhancement, which would presumably result from the low surface gravity of members of these solar metallicity clusters.

In addition, the BT–Settl Y -band flux is suppressed to some extent at lower gravity. However, this effect is not predicted by the Tucson or AMES models (with both models showing an increase in flux for lower gravity), and this trend is thus ambiguous when taking all models into consideration. Metallicity affects the K -band peak in a similar way to gravity, where increasing and decreasing metallicity causes K -band enhancement and suppression, respectively. Indeed, K -band fluxes may be quite sensitive to even small metallicity differences (e.g. Burgasser et al. 2002; Knapp et al. 2004; Liu, Leggett & Chiu 2007). K -band metallicity effects are well documented in the M subdwarfs (e.g. Leggett et al. 2000a) and have been explicitly attributed to the enhanced K -band peak in the T7.5 companion HD 3651B (Mugrauer et al. 2006; Burgasser 2007; Liu et al. 2007; Luhman et al. 2007). Furthermore, metallicity affects the Y -band flux peak significantly. This effect is also seen for the other models, although it is not clear how the Y -band peak should change. The Tucson and AMES models suggest that Y -band suppression could occur at higher metallicity, although the BT–Settl models suggest

that some enhancement may occur (at the expense of shorter wavelength flux).

We do not make direct comparison to the model predictions, but instead identify T dwarfs whose relative flux peak ratios and/or colours are unusual in the context of T dwarf properties typical of the solar neighbourhood. We compared the measurements of the T dwarfs with previous samples (from Golimowski et al. 2004; Knapp et al. 2004; Chiu et al. 2006), and found that most of the sample (11 out of 15) have ratios that appear consistent with the majority of solar neighbourhood T dwarfs. However, there are some notable exceptions.

(i) ULAS J0222–0024 and ULAS J0938–0011 appear to show Y_1 enhancement, suggestive of unusual metallicity. However, there is no evidence for an enhanced Y -band flux from the $Y - J$ colours, and the K/H ratio of ULAS J0222–0024 is not unusual. It is possible that the Y_1 band (but not the Y band) could be enhanced for these objects. This would be consistent with the BT–Settl model predictions for a high metallicity object (see Fig. 5), but the Y spectra of these objects are somewhat noisy and additional spectral coverage with good signal-to-noise ratio would be needed to properly confirm this.

(ii) ULAS J0958–0039 may show some Y -band and H -band enhancement, although the somewhat noisy nature of this object’s spectrum make this result rather tentative. However, it is supported by the relatively blue $Y - J$ colour of this object. Although note that the Y_1/J spectral ratio of this object is not unusual. Consideration of the models suggests that such an effect could arise from lower T_{eff} or unusual $[M/H]$, but it is not currently clear if either or both of these effects are responsible.

(iii) ULAS J1150+0949 shows strong Y and Y_1 suppression and also an enhanced K -band flux. The enhanced K/H ratio and relatively red $H - K$ colour is suggestive of low gravity. The suppressed Y -band flux for this object also points to low gravity when one considers the BT–Settl models. However, note that the Tucson and AMES models (which show no significant Y -band gravity sensitivity) could invoke an increase in metallicity to explain this Y -band suppression. While it seems simpler to require only one non-typical property to explain the unusual flux peak ratios, it is not possible to

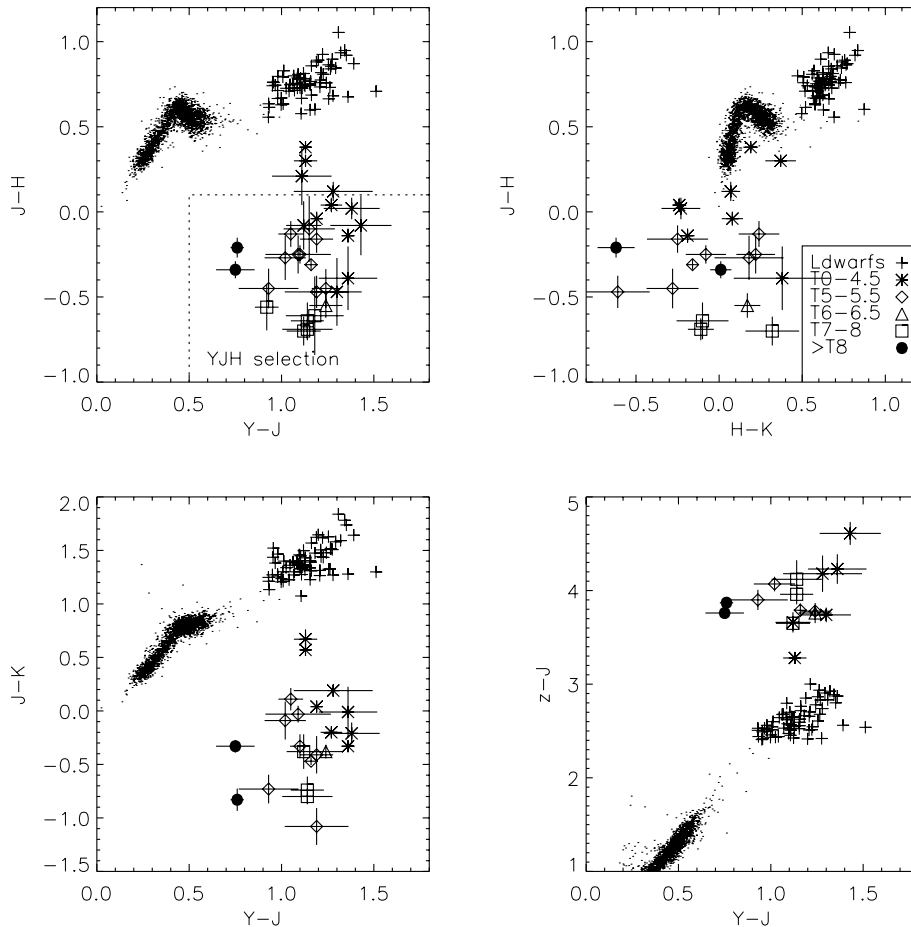


Figure 6. A series of two-colour diagrams showing the known LAS T dwarfs, including those first presented by Geballe et al. (2002), Kendall et al. (2007), Lodieu et al. (2007a), Warren et al. (2007b), Chiu et al. (2007) and this work.

make firm conclusions at this stage, in light of the model ambiguities. ULAS J0859+1010 also has suppressed Y_I flux and unusually red $H - K$ colour, and could have similar physical properties to ULAS J1150+0949.

(iv) ULAS J1303+0016 shows strong K -band suppression and very blue $H - K$ and $J - K$ colours, but has a normal Y -band flux peak. This is consistent with the predicted model trends for a high-gravity object.

(v) Finally, ULAS J1547+0053 shows typical Y_I/J and H/J spectral ratios, but has unusually red $J - K$ and $H - K$ colours. Like ULAS J1150+0949 this object may have low gravity, although it does not show suppressed Y_I flux.

We summarize the above discussion in the last column of Table 6, where we indicate possible non-typical properties that might explain the observed spectral morphology and colours.

5.1 Searching for the lowest T_{eff} objects

Fig. 6 shows the available colours of our new T dwarfs as well as other T dwarfs that have been discovered or recovered in the LAS (Geballe et al. 2002; Chiu et al. 2007; Kendall et al. 2007; Lodieu et al. 2007a; Warren et al. 2007b), including an additional T8+ object CFBDS0059, recently discovered using the Canada–France–Hawaii Telescope (Delorme et al. 2008) and independently identified in the LAS. Different T dwarf spectral types are indicated

with different symbols (see the key in the top right-hand plot). Also shown are the samples of DR2 L dwarf candidates (plus signs; see Section 2.1) and the sample of typical brighter sources from the LAS (points; see Section 2.1) for comparison. Our YJH selection box is indicated with a dotted line.

Examination of the plots shows several interesting features. For the blue T dwarfs (contained in our selection box) there is some evidence for a possible trend in $Y - J$ colour as one moves from the T0–4.5 dwarfs to the T5–8 dwarfs. This trend may be continuing into the T8+ objects, as suggested by the rather bluer colour of the T8.5 dwarfs ULAS J0034–0052 and CFBDS0059 (filled circles). The $J - H$ colours of T dwarfs generally get bluer out to spectral types of T8, although the two T8+ dwarfs do not have very blue $J - H$. The $H - K$ and $J - K$ colours show strong variations irrespective of spectral subclass, due presumably to variation in surface gravity and metallicity, and such variations appear to continue into the T8+ range. As such, these colours may not be strong indicators of T8+ types in themselves, although models do indicate that when combined with certain spectroscopic information (e.g. W_J index describing the width of the J -band peak) such colours (or flux ratios) can provide useful T_{eff} constraints (see fig. 7 of Warren et al. 2007b and fig. 6 of Delorme et al. 2008). The $z - J$ colour is clearly rather scattered for T dwarfs, and there is certainly no evidence in Fig. 6 for T dwarfs becoming redder in $z - J$ at lower T_{eff} . However, it is interesting to note that the $z - J$ colour of the two T8+ dwarfs is perhaps slightly bluer than other mid-late T dwarfs.

Although only two T8+ dwarfs are currently known, their colours suggests that $Y - J$ may be a particularly useful colour for identification. The $J - H$ colour shows no evidence so far for getting bluer beyond T8, however, this is based on only two objects, and we cannot rule out the possibility that the small number of T8+ dwarfs discovered so far could be unusual. A young (still contracting) brown dwarf for instance, would be brighter than an older counterpart of the same T_{eff} , and hence detectable to greater distance. This could provide an explanation as to why the first discoveries in this new T_{eff} range might have non-typical spectral properties. Clearly a larger sample of T8+ dwarfs is needed to properly understand their range of spectral properties. To this end, it could prove desirable to extend LAS searches for the lowest T_{eff} objects to even bluer $Y - J$ colours, and possibly redder $J - H$. Optical constraints (e.g. non-detections) would be particularly important as the near-infrared colours of candidates become more akin to those of hot stars, but the capabilities of UKIDSS and SDSS combine to give great potential for such searches.

6 T DWARF NUMBERS

In this section we discuss the sample of LAS T dwarfs identified thus far in DR1 and DR2, and place a magnitude limited constraint on T dwarf numbers in this 280 deg² of the LAS. We discuss various completeness issues, and make approximate corrections to the T dwarf statistics to account for these.

We first consider the completeness with which we have followed up candidates from DR1 and DR2. Overall we have followed up 82 per cent of all our $J \leq 19.5$ candidates (see Section 3). Nearly all those that still require follow-up are fainter than $J = 19$. Of the 44 initial candidates with $J \leq 19.0$, 42 have reliable classifications. The follow-up presented here combined with the previous observations reported by Chiu et al. (2008), Kendall et al. (2007), Lodieu et al. (2007a) and Warren et al. (2007b) have resulted in the discovery of 23 T dwarfs with $J - H \leq 0.1$ in the LAS DR2 sky. Of these, 22 T dwarfs have $J \leq 19.0$ (10 with $J < 18.5$ and 12 with $J = 18.5 - 19.0$). Since an extra half a magnitude depth should double the surveyed volume, it can be seen that our sample shows statistical evidence for a good level of completion down to $J = 19.0$.

The spread in colour of known T dwarfs means that our colour selection ($J - H \leq 0.1$) will thoroughly probe only certain ranges of T spectral class, and for some sub-type ranges a fraction of the T dwarfs will be missed. To assess the spectral type range that our colour selection probes, we used the population of optically selected SDSS T dwarfs² (to avoid near-infrared colour selection effects). SDSS T dwarf searches reach $z = 20.4$, and should thus be complete across the T range ($z - J \sim 3-4$) to $J \sim 16.4$. There are currently 19 SDSS T dwarfs with $J < 16.4$ and $J - H_{\text{MKO}} > 0.1$ which have been found in 6600 deg² of sky (see Chiu et al. 2006 and references therein). Amongst these, 14 have spectral type T0–2 and five have spectral type T2.5–3.5. None have a spectral type of T4 or greater. Correcting these numbers to a LAS $J = 19$ depth and sky coverage reveals that although we would not expect to have missed a significant number of $\geq T4$ dwarfs, we would expect to have missed ~ 21 T0–2 dwarfs and approximately eight T2.5–3.5 dwarfs. Clearly our search should be essentially complete for spectral types $\geq T4$, but a correction would be necessary if considering spectral type ranges that include earlier T dwarfs. Table 7 shows how this correction factor changes for different ranges of T spectral

Table 7. T dwarf sample statistics.

Spectral type range	No. in our $J < 19$ DR2 sky (280 deg ²)	Correction to include T dwarfs with $J - H > 0.1$	Final DR2 corrected number to $J = 19^a$
T0–T8.5	22–24	+95 ± 27 per cent	35 ± 9
T2.5–T8.5	22–24	+40 ± 15 per cent	24 ± 6
T4–T8.5	19–21	<10 per cent	17 ± 4

^aNumbers corrected to account for redder ($J - H > 0.1$) T dwarfs outside our selection, LAS photometric uncertainties, unresolved binarity for a BF in the 10–50 per cent range, spatial incompleteness and Malmquist/Eddington bias (see text).

class, and how the overall expected numbers of T dwarfs would be affected.

To take advantage of our good level of completeness and facilitate simple comparison with the theoretical predictions using the methods of Deacon & Hambly (2006), we specifically consider the spectral type range T4 and later. Allowing for the two outstanding candidates we place a constraint of 19–21 T4–T8.5 dwarfs with measured $J - H \leq 0.1$ and $J \leq 19$ in the LAS DR2 sky, and allow for an additional 10 per cent Poisson uncertainty on the upper limit to account for the limited statistical accuracy of our SDSS sample correction analysis.

To account for measurement uncertainties, we have estimated the number of $\geq T4$ dwarfs with intrinsic $J - H \leq 0.1$ whose colour may have been statistically scattered out of the selection region. To do this we estimated (for each $\geq T4$ dwarf discovered via YJH detection) the probability that $J - H$ colours could have been scattered sufficiently red-ward from the LAS measured value, taking into account the 1σ uncertainties on their measured colour. Probabilities were then summed, and our result suggests that we would only expect $\sim 1.5 \geq T4$ dwarfs to be missed in this way.

In addition, we account for some level of unresolved binarity amongst the LAS T dwarfs. Unresolved binaries will be brighter than a single T dwarf population, and could thus be found in a larger volume of sky. A correction is necessary if one wishes to compare T dwarf numbers with theoretical predictions for the total number of individual T dwarfs. Brown dwarf binaries are generally tight systems (e.g. <15 au; Reid et al. 2006) of approximately near equal mass components. A volume limited substellar binary fraction (BF) has been reported with values ranging from 10 to 50 per cent via open cluster photometry and high-resolution imaging (e.g. Burgasser et al. 2003; Pinfield et al. 2003; Lodieu et al. 2007b), where

$$\text{BF} = \frac{N_b}{N_b + N_s}, \quad (1)$$

N_b and N_s being the number of binary and single systems, respectively. If one makes the simplifying assumption of binary components of equal brightness (see Burgasser et al. 2003 for a more generalized conversion for a range of mass-ratio distributions; e.g. Allen 2007), then the relative number of binary and single systems in a magnitude-limited sample will be

$$\frac{N_b}{N_s} = \frac{2\sqrt{2}\text{BF}}{1 - \text{BF}}, \quad (2)$$

and the number of binary systems (compared to the total magnitude limited number of systems N_m) will be

$$N_b = \left[\frac{2\sqrt{2}}{2\sqrt{2} + (1/\text{BF}) - 1} \right] N_m. \quad (3)$$

² From the DwarfArchives.org site, <http://dwarfarchives.org>

For $\text{BF} = 10\text{--}50$ per cent, we thus estimate that 24–74 per cent of the sources in our magnitude limited sample could be unresolved binaries. Of these unresolved binary systems, only ~ 35 per cent ($1/2\sqrt{2} \times 100$ per cent) would be included in our $J \leq 19$ sample if the binary components were resolvable (i.e. if the combined binary J -band brightness is > 18.25 then the individual T dwarf components would have $J > 19$ and would be excluded from our sample). However, for the $J \leq 18.25$ unresolved binary systems, we must count both of the T dwarf components. We thus derive a binarity correction factor of 0.76–0.93 (for $\text{BF} = 10\text{--}50$ per cent, respectively) to correct our numbers to represent a magnitude limited sample of individual T dwarfs. Note that despite a wide range in BF , this binary correction factor has a relatively small range.

We also account for spatial incompleteness which can result from the way in which optical catalogues are used to inform candidate selection. In our initial selection, a nearby optical source might result in a candidate being rejected if it was close enough to masquerade as an optical counterpart, making the candidate appear too blue in its optical-to-infrared colour. This effectively decreases the search area by some fraction that is dependent on the source density and the search criteria used. We account for this with a correction factor (ϵ) that is the ratio of clear sky (unaffected by optical mismatches) to total sky considered (A_{tot}), and can be derived from probability analysis as

$$\epsilon = \left(1 - \frac{\sigma}{A_{\text{tot}}}\right)^N, \quad (4)$$

where σ is the area excluded by a single optical source and N is the number of optical sources in the area considered (see Burgasser 2001). For 1 deg^2 this reduces to $\epsilon = (1 - \sigma)^n$ where n is the number density of optical sources. Fig. 7 shows ϵ plotted against source density for our search of the LAS (solid line) as well as for previous searches of 2MASS (dashed line, e.g. Burgasser et al. 2004). The differences result from the different exclusion regions used, which extended out to 10 arcsec from any United States Naval Observatory (USNO)-A2.0 optical source for 2MASS searches, but only extend out to 2 arcsec from any SDSS source for our search of the LAS. The full effect of this incompleteness depends on the number density of optical sources in the regions of sky being considered, and this in turn is dependent on the galactic latitude. LAS DR2 extends across the $b = 20^\circ\text{--}80^\circ$ range, although is mostly concentrated in $b = 40^\circ\text{--}75^\circ$. The SDSS source number density ranges from $\sim 20\,000\text{--}$

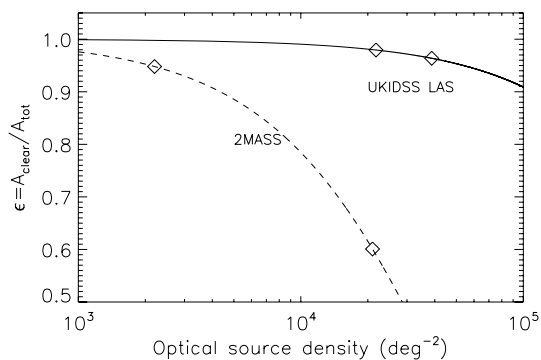


Figure 7. Predicted area corrections, $\epsilon = A_{\text{clear}}/A_{\text{tot}}$ for excluding regions around optical sources as a function of source density. The UKIDSS LAS exclusion regions comprise 2-arcsec radii circles centred on SDSS sources, and for comparison the 2MASS exclusion regions comprise 10-arcsec radii circles centred on USNO sources. The source densities inherent in our search and in previous 2MASS searches out of the plane are enclosed by open diamonds.

40 000 sources per square degree over the LAS DR2 sky (indicated by open diamonds in Fig. 7), and as can be seen, this results in a range of $\epsilon = 0.96\text{--}0.98$.

For the 2MASS comparison, despite the optical surveys being shallower than SDSS, the larger exclusion regions (with 10-arcsec radii) combined with the greater range of galactic latitude searched (reaching $|b| = 15$) result in the ϵ correction having a potentially much greater impact than it does for the LAS DR2 T dwarf sample. We chose to factor in a 3 per cent increase to our T dwarf numbers to account for this spatial incompleteness effect, but note that this small correction has no significant effect on our results.

In addition we account for Malmquist bias, which results from an intrinsic scatter in the M_J of T dwarfs. This scatter will cause the J -band magnitude limited sample to probe different volumes for any fixed spectral type. Those T dwarfs that are intrinsically brighter than average (for their type) will be sampled from a larger volume than those that are fainter. This will bias the mean M_J to brighter values, and effectively result in the overall sample coming from a larger volume than if the T dwarfs had a non-scattered M_J versus spectral type relation. Assuming a uniform space density, the fractional increase in the measured number of T dwarfs (ϕ) is given by

$$\frac{\Delta\phi}{\phi} = \left(\frac{0.6\sigma}{\log e}\right)^2 - \left(\frac{0.6\sigma^2}{\log e}\right) \frac{\phi'}{\phi}, \quad (5)$$

where σ is the rms dispersion (assuming a Gaussian distribution) of T dwarf absolute magnitudes, and ϕ' is the slope of the T dwarf luminosity function. The first term arises from the extra volume sampled due to the underestimated mean absolute magnitude, and the second term measures the effect of sampling the luminosity function at a slightly different absolute magnitude. We estimated σ using the sample of T dwarfs with parallax measurements presented by Liu et al. (2006) combined with their polynomial fit (M_J versus spectral type) to the single T dwarfs (ignoring known and possible unresolved binaries). When one considers only the subset of T dwarfs with spectral type $\geq \text{T4}$ (i.e. matched to the DR2 sample), the rms scatter from the best-fitting polynomial is $\sigma = 0.29$. Population synthesis results (e.g. Burgasser 2004) show that for $\alpha \leq 1$, $(\phi'/\phi) \lesssim 1/3$, and the second term in equation (5) is thus $\lesssim 4$ per cent. The first term in the equation represents a volume increase of 16 per cent, and clearly dominates over the second term. We thus made a Malmquist bias correction by decreasing our T dwarf numbers to account for a volume increase of 12–16 per cent.

Finally, we consider Eddington bias, which results from photometric uncertainty near the sample limit, since more T dwarfs will scatter into the sample from fainter magnitudes (i.e. greater distances, and a larger volume) than will scatter out of it. However, since we measured accurate follow-up photometry for the majority of our initial candidates (down to $J = 19.5$) before we imposed the $J = 19.0$ cut considered here, the effective scatter at the $J = 19$ limit will be small. We conservatively estimate this scatter to be $\sigma = 0.05$, and expect a resulting Eddington bias correction of no more than 0.5 per cent which is insignificant.

Our final magnitude limited T dwarf number constraints take account of the above corrections, and assumes Poisson uncertainties associated with sample sizes. We thus estimate that there are 17 ± 4 single $\geq \text{T4}$ dwarfs with $J < 19$ in the 280 deg^2 of DR2 sky. Table 7 also presents the number constraints derived using different lower limits for the spectral type range.

For comparison, we undertook a series of simulations based on those presented in Deacon & Hambly (2006). These were scaled to take into account the difference in size between the full LAS and

Table 8. Simulated late T dwarf (defined as those with $T_{\text{eff}} < 1300$ K) numbers for LAS DR2 (see text), for which we assumed input forms for the initial mass function (IMF) of $dn/dm \propto m^{-\alpha}$ or $dn/d(\log m) \propto m^{-x}$, and for the birth rate of $b(t) \propto e^{-\beta t}$.

Constant birth rate		
$\alpha = -1.0$	$x = -2.0$	15 ± 5
$\alpha = -0.5$	$x = -1.5$	25 ± 9
$\alpha = 0.0$	$x = -1.0$	44 ± 15
$\alpha = 0.5$	$x = -0.5$	57 ± 19
$\alpha = 1.0$	$x = 0.0$	119 ± 40
IMF with $\alpha = 0.0$ or $x = -1.0$		
$\beta = -0.1$		54 ± 18
$\beta = 0.0$		44 ± 15
$\beta = 0.1$		33 ± 11
$\beta = 0.2$		35 ± 12
$\beta = 1.0$		31 ± 11

DR2. The J -band depth limit was set to 19, and the Y -band depth limit to 20. This Y -band depth limit is actually 0.2 mag brighter than the 5σ detection limit, but this brighter limit effectively takes into account the known drop in detection completeness for $J = 19.7$ – 20.2 (Irwin, private communication). Unlike the Deacon & Hambly (2006) simulations we set no limit on the H -band detection, since objects not detected in the H -band will still be identified as part of our YJ selection. Furthermore, note that the Deacon & Hambly (2006) simulations used a normalization value of 0.0055 objects per cubic parsec in the mass range 0.1 – $0.09 M_{\odot}$ taken from Burgasser (2004). Here we use a normalization value of 0.0038 ± 0.0013 per cubic parsec calculated by Deacon, Nelemans & Hambly (2008). The results of these simulations are shown in Table 8, where the simulated late T dwarfs were defined as having $T_{\text{eff}} < 1300$ K. Mass function power-law indices α and x are also indicated ($x = \alpha - 1$), where the simulations assume functions of the form $dn/dm \propto m^{-\alpha}$ or $dn/d(\log m) \propto m^{-x}$ (following Chabrier 2003).

When comparing the observed number of T4–T8.5 dwarfs (from Table 7) to the predicted numbers in Table 8, and allowing for the associated uncertainties, it is clear that it is not possible to place a significant constraint on the birth rate. However, this comparison favours a range of α between -0.5 and -1.0 . Statistically our T dwarf numbers are also reasonably consistent (to within 1.5σ) with $\alpha = 0.0$. However, they are inconsistent with α of 0.5 and 1.0 at the 2.0 and 2.5σ level, respectively. This result is in reasonable agreement with the finding of Metchev et al. (2008), who performed a combined 2MASS and SDSS T dwarf search and derived a T dwarf space density that was most consistent with $\alpha = 0.0$ (although based on lower number statistics than here). However, L dwarf mass function constraints generally suggest values of α in the ~ 0.5 – 1.5 range (e.g. Reid et al. 1999; Allen et al. 2005; Cruz et al. 2007). The substellar mass functions of young open clusters are generally consistent with $\alpha \simeq 0.5$ (e.g. Caballero et al. 2007). However, a lognormal function also offers a reasonable fit to observation (see the Pleiades mass function in fig. 4 of Chabrier 2003). The slope of the lognormal mass function gets steeper as one decreases brown dwarf mass, and for $\sim 0.04 M_{\odot}$ the lognormal mass function slope is consistent with an $\alpha = 0.0$ power law.

A detailed comparison between mass function constraints from L and T dwarfs is beyond the scope of this paper, however, it may be that differences occur due to the T dwarfs probing a somewhat

lower mass range than the L dwarfs. This would suggest that a single power-law exponent is not optimal when describing the substellar mass function in the field. It may also be possible that the different measured α values result from issues with the evolutionary models used to convert between mass and magnitude. A greatly improved picture of the mass function will emerge from the LAS in the future as the survey area grows.

7 CONCLUSIONS AND FUTURE WORK

We have discussed our data base selection methods and the photometric follow-up that we performed to search for late T dwarfs and even cooler $T_{\text{eff}} = 400$ – 700 K objects in the UKIDSS LAS. These techniques have allowed us to make essentially complete follow-up of our candidates from DR1 and DR2 down to $J = 19$. We have also followed up some candidates from DR3 and a fraction of our fainter candidates from DR1 and DR2 (to $J = 19.5$). Using a variety of spectroscopic facilities we have measured the spectra of our best candidates, and have spectroscopically confirmed 15 new T dwarfs, bringing the total of number of confirmed LAS T dwarf discoveries to 28.

Compared to typical T dwarf properties, three of our new T dwarfs may have unusual metallicity, two may have relatively low surface gravity, and one may have higher than normal surface gravity. These assessments are based on comparisons between the spectral morphology and colours of the T dwarfs with theoretical models trends, and are thus somewhat speculative. However, all indications are that T dwarf spectra are quite sensitive to their physical properties, and it seems clear that a better understanding of these variations would have important implications for our ability to model T dwarf atmospheres, and potentially constrain (via spectroscopy) the mass, age and composition of T dwarf populations in the field (e.g. Pinfield et al. 2006). To this end, it would be very beneficial to identify T dwarfs whose properties could be constrained without the need to study their spectra. Both T dwarfs and L dwarfs of this type may be found in widely separated binary systems (e.g. Burgasser et al. 2000; Gizis et al. 2001; Wilson et al. 2001; Scholz et al. 2003; Pinfield et al. 2006; Luhman et al. 2007) for which the primary object can be used to constrain system age and composition.

The large volume (and large number of T dwarfs) probed by the LAS should yield many T dwarfs in such binary systems, and in this context we made a basic search for possible companions to all confirmed LAS T dwarfs out to a separation of ~ 10000 au (at the estimated distances in Table 5), by querying the SIMBAD astronomical data base (operated at CDS). We searched for neighbouring objects with either a measured spectral type, a parallax or a high proper motion, for which we could obtain distance constraints from either parallax or from spectral type and photometry. These distance constraints allowed us to rule out (as possible companions) all the neighbouring objects, by comparison with the distance constraints of the T dwarfs. However, proper motion measurements for all LAS T dwarfs would facilitate a more general search for common proper motion companions as the number of LAS T dwarfs grows, which could include white dwarf companions that can yield useful age constraints (e.g. Day-Jones et al. 2008) and are readily identified in SDSS (e.g. Gates et al. 2004; Kleinman et al. 2004; Eisenstein et al. 2006).

The number of blue ($J - H < 0.1$) LAS T dwarfs discovered with our methods shows statistical evidence for a good level of completeness down to $J = 19$. This builds on our previous work (e.g. Lodieu et al. 2007a) for which a good level of completion was only achieved to $J \sim 18.5$. The increased size of the

LAS T dwarf sample allowed us to place some statistical constraints on the substellar mass function. Indeed, there may be mounting evidence for a steepening (decreasing more rapidly with decreasing mass) substellar mass function in the field, with best-fitting α values of ~ 1 and between -1.0 and 0.0 for L and T dwarf populations, respectively. In any event, mass function constraints should be greatly improved by larger samples of LAS T dwarfs as the survey continues to grow. In addition, constraints on the brown dwarf birth rate should be attainable by building on the LAS L and early T dwarf searches mentioned briefly in Section 2.1 (e.g. fig. 3 of Deacon & Hambly 2006; fig. 10 of Burgasser 2004). For instance, a sample of ~ 100 L/T dwarfs per $\Delta T_{\text{eff}} = 100$ K range from 1100 to 1500 K (assuming a flat birth rate) would be capable of ruling out an exponential (e.g. $\tau_{\text{g}} \sim 5$ Gyr) birth rate at a $\sim 5\sigma$ level of significance. An appropriate sample of ~ 400 late L to mid T dwarfs could be identified in the full LAS to $J = 18.5$ (for a flat birth rate).

The discovery of the T8.5 dwarf ULAS J0034–0052 (Warren et al. 2007b) in the LAS absolutely demonstrates that UKIDSS is probing unexplored T_{eff} regimes beyond the previously known late T dwarfs. Having said this, parallax and adaptive optics measurements for this and other very late T dwarfs are important if we are to test for unresolved binarity and better constrain luminosity and T_{eff} . When comparing the colours of ULAS J0034–0052 with all available LAS T dwarfs, it is possible that a blue trend in $Y - J$ with decreasing T_{eff} may be present. The $J - H$ and $z - J$ colours might also change beyond T8, becoming slightly redder and bluer, respectively, although this needs further investigation. These spectral changes would be of great importance not only to our understanding of cool dwarf atmospheres, but also to the potential for finding such objects in the LAS. If it is the case that $T_{\text{eff}} = 400\text{--}700$ K objects become bluer in $Y - J$ and redder in $J - H$ than T8 dwarfs, it could be less problematic to identify such candidates to greater J -band depth in multiband searches of the combined LAS and SDSS data bases. Indeed, an evolving set of search criteria takes full advantage of the capabilities offered by large general surveys like UKIDSS and SDSS.

ACKNOWLEDGMENTS

Thanks to Adam Burgasser for a thorough and helpful referee's review. This work is based in part on data obtained as part of the UKIDSS. The UKIRT is operated by the Joint Astronomy Centre on behalf of the Science and Technology Facilities Council of the UK. Some of the data reported here were obtained as part of the UKIRT Service Programme. Based on observations obtained at the Gemini Observatory, which is operated by the Association of Universities for Research in Astronomy, Inc., under a cooperative agreement with the NSF on behalf of the Gemini partnership: the National Science Foundation (United States), the Science and Technology Facilities Council (United Kingdom), the National Research Council (Canada), CONICYT (Chile), the Australian Research Council (Australia), CNPq (Brazil) and SECYT (Argentina). Based in part on data collected at the Subaru Telescope, which is operated by the National Astronomical Observatory of Japan. SKL's research is supported by the Gemini Observatory. Based on observations made with the TNG operated on the island of La Palma by the Fundacin Galileo Galilei of the INAF (Istituto Nazionale di Astrofisica) at the Spanish Observatorio del Roque de los Muchachos of the Instituto de Astrofisica de Canarias. This publication makes use of data products from the 2MASS, which is a joint project of the University of Massachusetts and the Infrared Processing and Analysis Center/California Institute of Technology, funded by

the National Aeronautics and Space Administration and the National Science Foundation. Funding for the SDSS and SDSS-II has been provided by the Alfred P. Sloan Foundation, the Participating Institutions, the National Science Foundation, the US Department of Energy, the National Aeronautics and Space Administration, the Japanese Monbukagakusho, the Max Planck Society, and the Higher Education Funding Council for England. The SDSS Web Site is <http://www.sdss.org/>. The SDSS is managed by the Astrophysical Research Consortium for the Participating Institutions. The Participating Institutions are the American Museum of Natural History, Astrophysical Institute Potsdam, University of Basel, University of Cambridge, Case Western Reserve University, University of Chicago, Drexel University, Fermilab, the Institute for Advanced Study, the Japan Participation Group, Johns Hopkins University, the Joint Institute for Nuclear Astrophysics, the Kavli Institute for Particle Astrophysics and Cosmology, the Korean Scientist Group, the Chinese Academy of Sciences (LAMOST), Los Alamos National Laboratory, the Max-Planck-Institute for Astronomy (MPIA), the Max-Planck-Institute for Astrophysics (MPA), New Mexico State University, Ohio State University, University of Pittsburgh, University of Portsmouth, Princeton University, the United States Naval Observatory and the University of Washington. The William Herschel Telescope is operated on the island of La Palma by the Isaac Newton Group in the Spanish Observatorio del Roque de los Muchachos of the Instituto de Astrofisica de Canarias. This research has benefited from the M, L and T dwarf compendium housed at DwarfArchives.org and maintained by Chris Gelino, Davy Kirkpatrick and Adam Burgasser. This research has made use of the SIMBAD data base, operated at CDS, Strasbourg, France.

REFERENCES

- Allard F., Hauschildt P., Alexander D., Tamanai A., Schweitzer A., 2001, *ApJ*, 556, 357
 Allen P. R., 2007, *ApJ*, 668, 492
 Allen P. R., Koerner D. W., Reid I. N., Trilling D. E., 2005, *ApJ*, 625, 385
 Baffa C. et al., 2001, *A&A*, 378, 722
 Baraffe I., Chabrier G., Barman T. S., Allard F., Hauschildt P. H., 2003, *A&A*, 402, 701
 Becklin E. E., Zuckerman B., 1988, *Nat*, 336, 656
 Burgasser A. J. et al., 2000, *ApJ*, 531, L57
 Burgasser A. J., 2001, PhD thesis, California Institute of Technology
 Burgasser A. J., 2004, *ApJS*, 155, 191
 Burgasser A. J., 2007, *ApJ*, 658, 617
 Burgasser A. J. et al., 2002, *ApJ*, 564, 421
 Burgasser A. J., Kirkpatrick J. D., Reid I. N., Brown M. E., Miskey C. L., Gizis J. E., 2003, *ApJ*, 586, 512
 Burgasser A. J., McElwain M. W., Kirkpatrick J. D., Cruz K. L., Tinney C. G., Reid I. N., 2004, *AJ*, 127, 2856
 Burgasser A. J., Kirkpatrick J. D., Cruz K. L., Reid I. N., Leggett S. K., Liebert J., Burrows A., Brown M. E., 2006a, *ApJS*, 166, 585
 Burgasser A. J., Geballe T. R., Leggett S. K., Kirkpatrick J. D., Golimowski D. A., 2006b, *ApJ*, 637, 1067 (B06)
 Burgasser A. J., Burrows A. J., Kirkpatrick J. D., 2006c, *ApJ*, 639, 1095
 Burrows A., Sudarsky D., Lunine J. I., 2003, *ApJ*, 596, 587
 Burrows A., Sudarsky D., Hubeny I., 2006, *ApJ*, 640, 1063
 Caballero J. A. et al., 2007, *A&A*, 470, 903
 Carpenter J. M., 2001, *AJ*, 121, 2851
 Casali M. et al., 2007, *A&A*, 467, 777
 Casewell S. L., Dobbie P. D., Hodgkin S. T., Moraux E., Jameson R. F., Hambly N. C., Irwin J., Lodieu N., 2007, *MNRAS*, 378, 1131
 Chabrier G., 2003, *PASP*, 115, 763
 Chiu K., Fan X., Leggett S. K., Golimowski D. A., Zheng W., Geballe T. R., Schneider D. P., Brinkmann J., 2006, *AJ*, 131, 2722
 Chiu K. et al., 2008, *MNRAS*, 385, L53

- Cruz K. L. et al., 2007, *AJ*, 133, 439
Dahn C. C. et al., 2002, *AJ*, 124, 1170
Day-Jones A. C. et al., 2008, *MNRAS*, 388, 838
Deacon N. R., Hambly N. C., 2006, *MNRAS*, 371, 1722
Deacon N. R., Nelemans G., Hambly N. C., 2008, *A&A*, 486, 283
Dye S. et al., 2006, *MNRAS*, 372, 1227
Eisenstein D. J. et al., 2006, *ApJS*, 167, 40
Elias J. H., Joyce R. R., Liang M., Muller G. P., Hilman E. A., George J. R., 2006, *Proc. SPIE*, 6269, 138
Epchtein N. et al., 1997, *Messenger*, 87, 27
Folkes S. L., Pinfield D. J., Kendall T. R., Jones H. R. A., 2007, *MNRAS*, 378, 901
Gates E. et al., 2004, *ApJ*, 612, L129
Geballe T. R., Saumon D., Leggett S. K., Knapp G. R., Marley M. S., Lodders K., 2001, *ApJ*, 556, 373
Geballe T. R. et al., 2002, *ApJ*, 564, 466
Gizis J. E., Kirkpatrick J. D., Burgasser A. J., Reid I. N., Monet D. G., Liebert J., Wilson J. C., 2001, *ApJ*, 551, L163
Golimowski D. A. et al., 2004, *AJ*, 127, 3516
Hambly N. C. et al., 2008, *MNRAS*, 384, 637
Hauschildt P. H., Baron E., 1999, *J. Comput. Appl. Math.*, 102, 41
Hewett P., Warren S. J., Leggett S. K., Hodgkin S. T., 2006, *MNRAS*, 367, 454
Hodapp K. W. et al., 2003, *PASP*, 115, 1388
Irwin M. J. et al., 2004, *Proc. SPIE*, 5493, 411
Kendall T. R. et al., 2007, *A&A*, 466, 1059
Kirkpatrick J. D., 2005, *ARA&A*, 43, 195
Kirkpatrick J. D., Henry T. J., Liebert J., 1993, *ApJ*, 406, 701
Kirkpatrick J. D. et al., 1999, *ApJ*, 519, 802
Kirkpatrick J. D. et al., 2000, *AJ*, 120, 447
Kleinman S. J. et al., 2004, *ApJ*, 607, 426
Knapp G. R. et al., 2004, *AJ*, 127, 3553
Knutson H. A. et al., 2007, *Nat*, 447, 183
Kobayashi N. et al., 2000, *Proc. SPIE*, 4008, 1056
Kucinkas A. et al., 2005, *A&A*, 442, 281
Kucinkas A. et al., 2006, *A&A*, 452, 1021
Lawrence A. et al., 2007, *MNRAS*, 370, 1599
Leggett S. K. et al., 2000a, *ApJ*, 535, 965
Leggett S. K. et al., 2000b, *ApJ*, 536, L35
Leggett S. K. et al., 2006, *MNRAS*, 373, 781
Leggett S. K. et al., 2007, *ApJ*, 667, 537
Liu M. C. et al., 2006, *ApJ*, 647, 1393
Liu M. C., Leggett S. K., Chiu K., 2007, *ApJ*, 660, 1507
Lodieu N. et al., 2007a, *MNRAS*, 379, 1423
Lodieu N., Dobbie P. D., Deacon N. R., Hodgkin S. T., Hambly N. C., Jameson R. F., 2007b, *MNRAS*, 380, 712
Looper D. L., Kirkpatrick J. D., Burgasser A. J., 2007, *AJ*, 134, 1162
Luhman K. et al., 2007, *ApJ*, 654, 570
Manchado A. F. et al., 1998, *Proc. SPIE*, 3354, 448
Marley M. S., 2007, *AAS*, 210, 9604
Marley M. S., Seager S., Saumon D., Lodders K., Ackerman A. S., Freedman R. S., Fan X., 2002, *ApJ*, 568, 335
Masana E., Jordi C., Ribas I., 2006, *A&A*, 450, 735
Metchev S. A., Kirkpatrick J. D., Berriman G. B., Looper D., 2008, *ApJ*, 676, 1281
Mugrauer M., Seifahrt A., Neuhauser R., Mazeh T., 2006, *MNRAS*, 373, L31
Nakajima T., Oppenheimer B. R., Kulkarni S. R., Golimowski D. A., Matthews K., Durrance S. T., 1995, *Nat*, 378, 463
Pinfield D. J., Dobbie P. D., Jameson R. F., Steele I. A., Jones H. R. A., Katsiyannis A. C., 2003, *MNRAS*, 342, 1241
Pinfield D. J. et al., 2006, *MNRAS*, 368, 1281
Ramsay Howat S. K. et al., 2004, *Proc. SPIE*, 5492, 1160
Reid I. N. et al., 1999, *ApJ*, 521, 613
Reid I. N., Lewitus E., Allen P. R., Cruz K. L., Burgasser A. J., 2006, *AJ*, 132, 891
Roche P. F. et al., 2003, *Proc. SPIE*, 4841, 901
Saumon D., Marley M. S., Lodders K., Freeman R. S., 2003, in Eduardo Martin, ed., *Proc. IAU Symp.* 211, ASP Conf. Ser. Vol. 345, Brown Dwarfs
Saumon D., Marley M. S., Cushing M. C., Leggett S. K., Roellig T. L., Lodders K., Freedman R. S., 2006, *ApJ*, 647, 552
Saumon D. et al., 2007, *ApJ*, 656, 1136
Scholz R. D., McCaughrean M. J., Lodieu N., Kuhlbrodt B., 2003, *A&A*, 398, L29
Skrutskie M. F. et al., 2006, *AJ*, 131, 1163
Tinney C. G., Burgasser A. J., Kirkpatrick J. D., 2003, *AJ*, 126, 975
Tinney C. G., Burgasser A. J., Kirkpatrick J. D., McElwain M. W., 2005, *AJ*, 130, 2326
Tokunaga A. T., Simons D. A., Vacca W. D., 2002, *PASP*, 114, 180
Tsuji T., Nakajima T., Tanagisawa K., 2004, *ApJ*, 607, 511
Vrba F. J. et al., 2004, *AJ*, 127, 2948
Warren S. J., Hewett P., 2002, in ASP Conf. Ser. Vol. 283. Astron. Soc. Pac., San Francisco, p. 369
Warren S. J. et al., 2007a, *MNRAS*, 375, 213
Warren S. J. et al., 2007b, *MNRAS*, 381, 1400
Warren S. J. et al., 2007c, preprint (astro-ph/0703037)
Wilson J. C., Kirkpatrick J. D., Gizis J. E., Skrutskie M. F., Monet D. G., Houck J. R., 2001, *AJ*, 122, 1989
York D. G. et al., 2000, *AJ*, 120, 1579
Zapatero-Osorio M. R. et al., 2008, *A&A*, 477, 895

This paper has been typeset from a $\text{\TeX}/\text{\LaTeX}$ file prepared by the author.